AD-A267 543

JMENTATION PAGE

Form Approved
OMB No. 0704-0188

1. AGENCY USE ONLY (Leave blank)	2. REPORT DATE	3. REPORT TYPE AND DATES COVERED
	May 1993	THESIS/DISSERTATION

4. TITLE AND SUBTITLE
The Specific Heat of Titanium Disilicide

5. FUNDING NUMBERS

6. AUTHOR(S)
1Lt William Kevin Sylla

7. PERFORMING ORGANIZATION NAME(S) AND ADDRESS(ES)
AFIT Student Attending:State Univ of New York at Binghamton

8. PERFORMING ORGANIZATION REPORT NUMBER
AFIT/CI/CIA- 93-094

9. SPONSORING/MONITORING AGENCY NAME(S) AND ADDRESS(ES)
DEPARTMENT OF THE AIR FORCE
AFIT/CI
2950 P STREET
WRIGHT-PATTERSON AFB OH 45433-7765

10. SPONSORING/MONITORING AGENCY REPORT NUMBER

11. SUPPLEMENTARY NOTES

12a. DISTRIBUTION/AVAILABILITY STATEMENT
Approved for Public Release IAW 190-1
Distribution Unlimited
MICHAEL M. BRICKER, SMSgt, USAF
Chief Administration

12b. DISTRIBUTION CODE

13. ABSTRACT (Maximum 200 words)

14. SUBJECT TERMS	15. NUMBER OF PAGES 66
	16. PRICE CODE

17. SECURITY CLASSIFICATION OF REPORT	18. SECURITY CLASSIFICATION OF THIS PAGE	19. SECURITY CLASSIFICATION OF ABSTRACT	20. LIMITATION OF ABSTRACT

Author: William Kevin Sylla, 1 Lt. USAF
Title: The Specific Heat of Titanium Disilicide
Date: 1993
Pages: 66
Degree: Master of Science
Institution: State University of New York at Binghamton

Abstract

Titanium disilicide is a promising candidate for use in the circuitry of the next generation of micro - electronics. The fabrication techniques used by the electronics industry require accurate thermodynamic data. We have therefore undertaken the measurement of the specific heat of $TiSi_2$.

The titanium disilicide alloy has been produced and characterized. The lattice parameters of $TiSi_2$ have been found to be: $a = 8.2607 \pm 0.0004$ Å, $b = 4.7967 \pm 0.0003$ Å, and $c = 8.545 \pm 0.002$ Å by x - ray diffractometry. The specific heat of titanium disilicide has been measured from 100 K to 500 K by means of differential scanning calorimetry. These data show good agreement with accepted specific heat theory, following the general shape of a Debye curve and approaching a Dulong - Petit value. From these data a Debye temperature of 510 ± 80 K has been graphically approximated.

The methodology of specific heat measurements using differential scanning calorimetry has been reviewed.

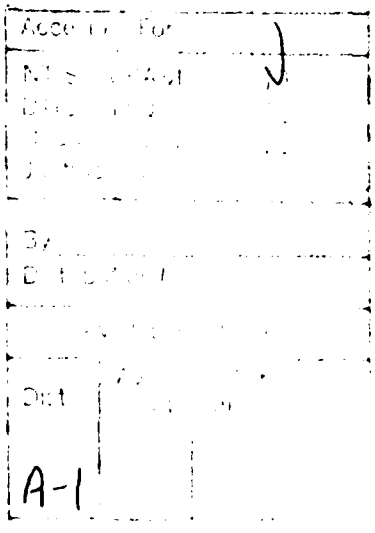

THE SPECIFIC HEAT OF TITANIUM DISILICIDE

BY

1 LT. WILLIAM KEVIN SYLLA

B.S., UNITED STATES AIR FORCE ACADEMY, 1990

THESIS
Submitted in partial fulfillment of the requirements for
the degree of Master of Science in Physics
in The Graduate School of the
State University of New York
at Binghamton
1993

Accepted in partial fulfillment of the requirements for
the degree of Master of Science in Physics
in The Graduate School of the
State University of New York
at Binghamton

Eric J. Cotts
Physics Department _____ May 17, 1993

Clifford A. Myers
Chemistry Department _____ May 17, 1993

Robert L. Pompi
Physics Department _____ May 17, 1993

Noel K. Yeh
Physics Department _____ May 17, 1993

Abstract

Titanium disilicide is a promising candidate for use in the circuitry of the next generation of micro - electronics. The fabrication techniques used by the electronics industry require accurate thermodynamic data. We have therefore undertaken the measurement of the specific heat of $TiSi_2$.

The titanium disilicide alloy has been produced and characterized. The lattice parameters of $TiSi_2$ have been found to be: $a = 8.2607 \pm 0.0004$ Å, $b = 4.7967 \pm 0.0003$ Å, and $c = 8.545 \pm 0.002$ Å by x - ray diffractometry. The specific heat of titanium disilicide has been measured from 100 K to 500 K by means of differential scanning calorimetry. These data show good agreement with accepted specific heat theory, following the general shape of a Debye curve and approaching a Dulong - Petit value. From these data a Debye temperature of 510 ± 80 K has been graphically approximated.

The methodology of specific heat measurements using differential scanning calorimetry has been reviewed.

Acknowledgments

I would like to thank the physics department faculty, staff, and students for the guidance and help that I have received in preparation of this thesis. I would especially like to thank Professor Eric Cotts, my advisor, for his dedication, insights and encouragement.

I would also like to thank Professor Clifford Myers and Dr. Robert Kematick for sharing their equipment and expertise.

Thank you to the members of my committee. Your time spent reviewing this thesis is appreciated.

Thanks to my fellow lab mates and departmental staff.

Lastly, I would like to thank my wife, Monica.

Contents

List of Tables

List of Figures

Introduction

As micro - electronic technology advances, the circuitry on computer chips become smaller and smaller. As these circuits become smaller, the characterization of these micro-devices and the interconnects among them becomes more important. Although the materials used for interconnects today have exceptional conductive properties, they also have a tendency to react with the silicon chips on which they are deposited. These reactions impede device performance and make the characterization of these circuits extremely difficult. An example of a material that is commonly used on today's microchips is aluminum. It has a low resistivity, 2.7 $\mu\Omega$cm, but because of its low alloying temperature with silicon (577 C), there is a tendency for silicon to electromigrate into the aluminum.[1] As the physical size of interconnect becomes smaller, this electromigration will have more pronounced effects, causing less than reliable circuits. Because of difficulties such as this, the materials used in today's micro - electronic chips may not be suitable for use in tomorrow's.

Titanium disilicide, $TiSi_2$, has a relatively low resistance (12.4 $\mu\Omega$cm), and because it is a line compound in the Ti - Si phase diagram, it is in thermodynamically stable state when deposited on a silicon chip. For these reasons it is one material being considered for use as interconnects in the next generation of electronic devices. One of the most promising methods of creating these interconnects is chemical vapor deposition, CVD.[2]

CVD is a process by which material is deposited on a substrate due to chemical reactions on or near the surface. A simplified picture of a CVD reactor is shown in Fig. 1. The type of material deposited on the substrate is a function of temperature, pressure and molar ratios among the reactants. The position on the substrate where the deposition occurs is called the selectivity. The selectivity is controlled by either using a patterned substrate or by heating only the appropriate positions of the substrate.[2]

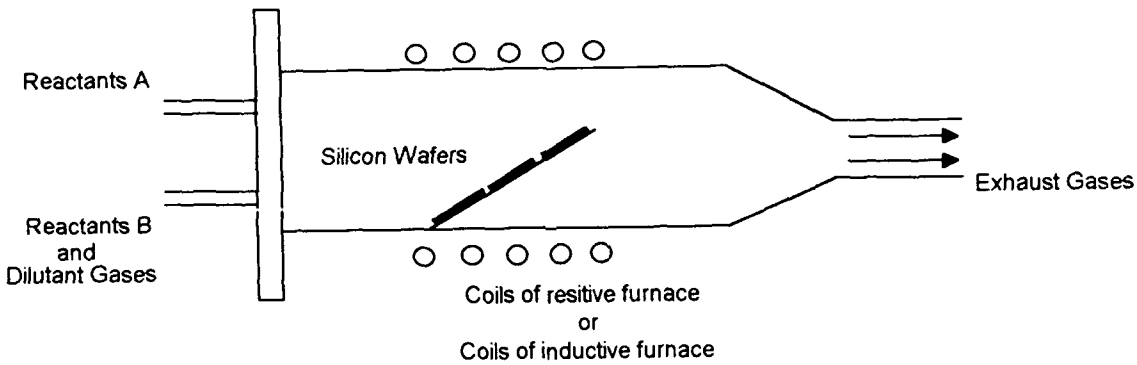

Figure. 1

Simplified schematic of a CVD reactor. The reacting chemicals are fed into the reactor through different feed lines. Once inside, the flows are mixed and react to deposit a film on the substrate. In this case the substrate is a silicon chip.

Several chemical processes can be implemented for the CVD of $TiSi_2$ on to a silicon substrate. One such reaction is:

$$TiCl_4\ (g) + 3Si\ (s) \rightarrow TiSi_2\ (s) + SiCl_4\ (g). \qquad \text{Eq. 1}$$

Here there is a large consumption of the substrate, about 925 nm of Si substrate for a 535 nm $TiSi_2$ film.[3] This is undesirable for the production of shallow interconnects. This consumption can be reduced by introducing hydrogen which reacts with the chlorine. For this set of reactants the equation is:

$$TiCl_4\ (g) + 2H_2\ (g) + 2Si\ (s) \rightarrow TiSi_2\ (s) + 4HCl\ (g). \qquad \text{Eq. 2}$$

Here the consumption is about 280 nm of Si for a 264 nm layer of $TiSi_2$.[3] The most promising way to eliminate substrate consumption is by introducing another source of silicon. For example, silane gas,

$$TiCl_4\ (g) + 2SiH_4\ (s) \rightarrow TiSi_2\ (s) + 4HCl\ (g) + 2H_2. \qquad \text{Eq. 3}$$

Despite the introduction of another silicon-carrying reactant, consumption of silicon substrate will still occur if the duration of this reaction is not closely monitored.[4] There is a drawback to introducing silane as a reactant; the deposition is not as selective because there is less dependence on the silicon in the substrate.[4]

Modeling a CVD Reactor:

In order for a given, specific material to be deposited in a CVD reactor, the material should constitute the equilibrium state of the thermodynamic system. In this situation, the system is a CVD reactor. For a given temperature, molar ratios, and total pressure inside the reactor, there will be an equilibrium state. This equilibrium state will have the lowest Gibbs free energy. Therefore, the equilibrium state for any given set of precursors can be predicted by minimizing the Gibbs free energy for the entire system. The change in the free energy for any given reaction at a given temperature is :

$$\Delta G_T^o = \Delta H_T^o - T\Delta S_T^o, \qquad \text{Eq. 4}$$

where ΔH_T^o, the change in the standard molar enthalpy for the reaction is:

$$\Delta H_T^o = \sum_i \nu_i \Delta_f H_i^o(products) - \sum_j \nu_j \Delta_f H_j^o(reactants), \qquad \text{Eq. 5}$$

and ΔS_T^o, the change in the standard molar entropy for the reaction is:

$$\Delta S_T^o = \sum_i \nu_i S_i^o(products) - \sum_j \nu_j S_j^o(reactants). \qquad \text{Eq. 6}$$

In the two previous equations ν_i denotes the number of moles of each of the products and ν_j denotes the number of moles of the reactants. The standard molar enthalpy, $\Delta_f H^o$, and the standard molar entropy, S^o, can be found in tables of thermodynamic properties, if these properties have been measured.

If $\Delta_f H^o$ and S^o are known at 298°C, the change in the Gibbs free energy for the reaction can be found for different temperatures if the forms of the specific heat functions for the various products and reactants are known. To make this possible Eq. 4 is rewritten as:

$$\Delta G_T^o = \Delta H_{298}^o - T\Delta S_{298}^o + (\Delta H_T^o - \Delta H_{298}^o) - T(\Delta S_T^o - \Delta S_{298}^o), \qquad \text{Eq. 7}$$

where the quantities $(\Delta H_T^o - \Delta H_{298}^o)$ and $(\Delta S_T^o - \Delta S_{298}^o)$ can be obtained by integrating the difference between the specific heat functions of the products and reactants.

$$(\Delta H_T^o - \Delta H_{298}^o) = \int_{298}^{T_2} \Delta C_P^o \, dT. \qquad \text{Eq. 8}$$

For the second,

$$(\Delta S_T^o - \Delta S_{298}^o) = \int_{298}^{T_2} \frac{\Delta C_P^o}{T} dT. \qquad \text{Eq. 9}$$

The change in the specific heat, ΔC_P^o, for the reaction can be written as:

$$\Delta C_P^o = \sum_i \nu_i C_{P_i}^o(products) - \sum_j \nu_j C_{P_j}^o(reactants). \qquad \text{Eq. 10}$$

In order to predict what is going to happen inside a CVD reactor, Eq. 7 must be written for all possible reactions among any of the input species. The Gibbs free energy for the system may then be minimized, with respect to these reactions, for the given temperature and pressure. The products of the reactions that give the lowest Gibbs free

energy should theoretically be the output of the CVD reactor in the absence of kinetic factors.

To perform these calculations, the thermodynamic properties of all the reactants and products: standard molar enthalpy, standard molar entropy and the specific heat; must be accurately known. Because the entropy and enthalpy values can be found by integrating the specific heat function, measurements of specific heat are highly valuable.

Up to this date only a small amount of research has been done on the thermodynamic properties of the titanium silicides. Reported values for specific heat are extremely limited and have been brought into question.[5,6,7,8] The requirement of accurate thermodynamic data for all the titanium silicides for use in modeling CVD processes is our impetus for studying the specific heat of $TiSi_2$.

Specific heat:

A very basic definition for the molar specific heat of a substance is the amount of heat required to raise one mole of the substance one degree Kelvin. A more precise definition, rooted in thermodynamics, is that the molar specific heat of a substance is the change in the enthalpy, with respect to temperature, of the substance at a constant pressure.

$$C_P = \left(\frac{\partial H}{\partial T}\right)_P \qquad \text{Eq. 11}$$

In 1819, Dulong and Petit reported an empirical observation about the specific heats of solids: all solid elements display a room temperature specific heat of about 25 J/moles * K.[9] Fifty - two years later Boltzman was able to provide a theoretical basis for this value, based upon what was to become know as Maxwell - Boltzman statistics.[10] From this theory, and the assumption that the energy functions of a particle are quadratic in nature, Boltzman was able to derive the equipartion of energy.

A particle will possess $\frac{1}{2}k_BT$ units of energy for each of its degrees of freedom. In a solid material the motions of a point particle are confined to vibrations. Each vibration

has six degrees of freedom: three due the translational energy of the particle and three due to its potential energy. Since each of these six degrees of freedom will possess $\frac{1}{2}k_BT$ units of energy, the internal energy of a solid material consisting of N particles is:

$$U = 3Nk_BT. \qquad \text{Eq. 12}$$

Differentiating with respect to T, at a constant volume, and dividing by Avogadro's number will give $C_V = 3R = 24.94\ Joules/(mole*Kelvin)$.

While this theory gave reasonable results for room temperature values, it could not explain the diminished value of the specific heat of solids in the lower temperature ranges. Einstein was able to explain this phenomena by considering the particles in a solid quantized oscillators. His assumption was that all of the oscillators in a solid have the same frequency, ω_E. The result he obtained gave the general shape of the of the specific heat curve we know today.

$$C_V^{Einstein} = 3N k_B \left(\frac{\hbar\omega_E}{k_B T}\right)^2 \frac{e^{\hbar\omega_E/k_B T}}{\left[e^{\hbar\omega_E/k_B T} - 1\right]^2} \qquad \text{Eq. 13}$$

If the Einstein temperature of a solid is defined as, $\Theta_E \equiv \hbar\omega_E/k_B$, a plot of C_V vs. T/Θ_E will have the form of Fig. 2.

Although the Einstein approximation will give the general shape of the specific heat curve, it does not accurately predict the values of C_V near absolute zero. This failure is due to the overly simple approximation made by Einstein. His assumption that each oscillator had the same frequency meant that there could be no coupling between the oscillators. In 1912 Debye made a little less simple assumption. He assumed the velocity of sound to be constant in the material. This assumption means that ω, the vibrational frequency is now proportional to $k = 2\pi/\lambda$, the wave number of the vibrations. The proportionality constant is v, the speed of sound: $\omega = vk$. Based upon this assumption the following specific heat function can be derived:

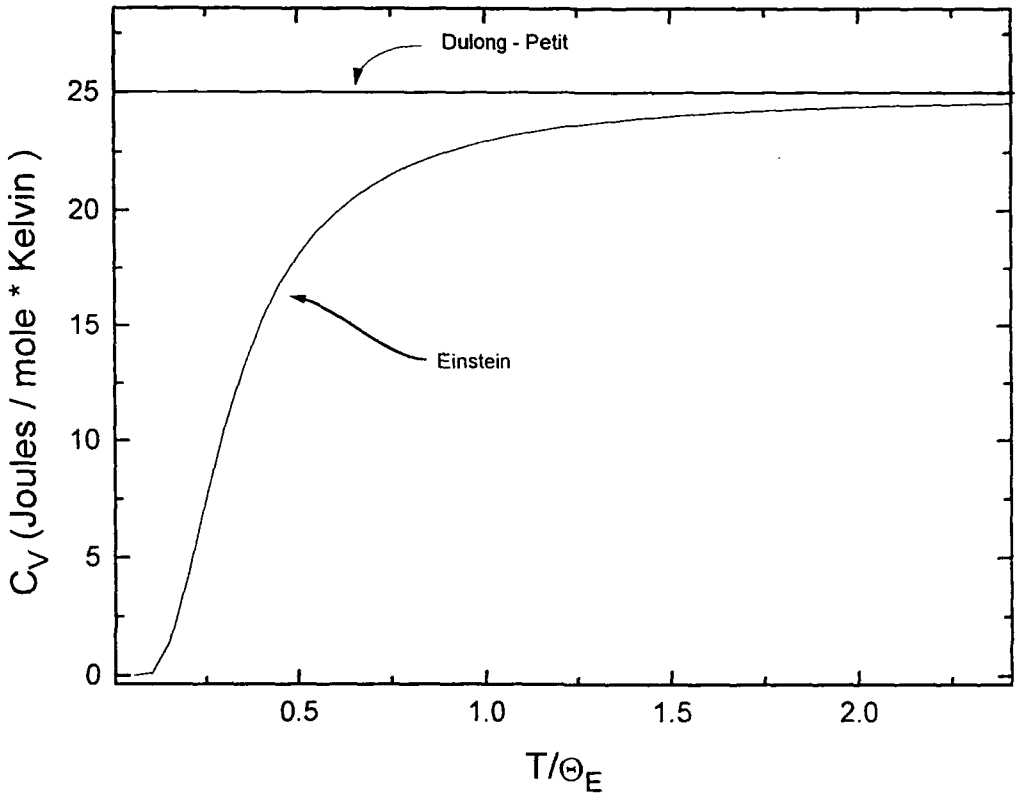

Figure. 2

The Einstein heat capacity of solid matter vs. T/Θ_E where $\Theta_E = \hbar\omega/k_B$. Also plotted is the Dulong - Petit value. Einstein's theory was the first to explain the low temperature shape of C_V curve. It can be seen that this model does predict the correct value of C_V for room temperature. Although it predicts the correct shape of the C_V curve is does not predict C_V accurately at temperatures near absolute zero.

$$C_V = \frac{3V\hbar^2}{2\pi^2 v^3 k_B T^2} \int_0^{\omega_D} d\omega \frac{\omega^4 e^{\hbar\omega/k_B T}}{\left(e^{\hbar\omega/k_B T} - 1\right)^2} \qquad \text{Eq. 14}$$

The Debye temperature can be defined as follows:

$$\theta_D = \frac{\hbar v}{k_B} \cdot \left(\frac{6\pi^2 N}{V}\right)^{1/3} \qquad \text{Eq. 15}$$

where V is the volume of the unit cell and N is the total number of vibration modes. Fig. 3 is a plot of C_V vs. T/Θ_D.

Estimation of Specific Heat (Kopp's Rule):

Although the value of the specific heat of $TiSi_2$ near room temperature has not been experimentally established; a value, based on the measured heat capacities of chromium disilicide, cobalt disilicide, and vanadium disilicide[11] can be estimated. The general rule for the estimation of specific heat values is known as Kopp's rule. Kopp's rule states that specific heat of a solid compound is the sum of the heat capacities of its component elements. Because the downturn points of the specific heat plots for different materials are not equal, this approximation is only valid for the Dulong - Petit region. The estimate of titanium disilicide's specific heat from that of chromium disilicide can be performed as follows.

$$C_P(TiSi_2) = C_P(CrSi_2) - C_P(Cr) + C_P(Ti). \qquad \text{Eq. 16}$$

Although the specific heat of $TiSi_2$ has not be experimentally established, Kubachewski has published a value based upon the data for the silicides listed above[12]. Fig. 4 is a plot of Kubachewski's estimation, as well the values estimated by Kopp's rule from the specific heat data of the silicides listed above. A fourth estimate was made based solely on the specific heats of Ti and Si. Also plotted are the experimental data of Golutvin. It can be seen from the graph that there is a large discrepancy between the estimated values and the experimental data of Golutvin.

Although the specific heat of $TiSi_2$ at high temperature can be approximated, this approximation does not agree with the only measured values of this property. Therefore more experimental data is required to determine which is a closer representation of the specific heat of $TiSi_2$ for room temperature and above. Also, due to the different downturn points of the various specific heat curves, there is no way to estimate values below room temperature. Therefore the future of the micro - electronics industry may hinge upon accurate measurement of the specific heat $TiSi_2$.

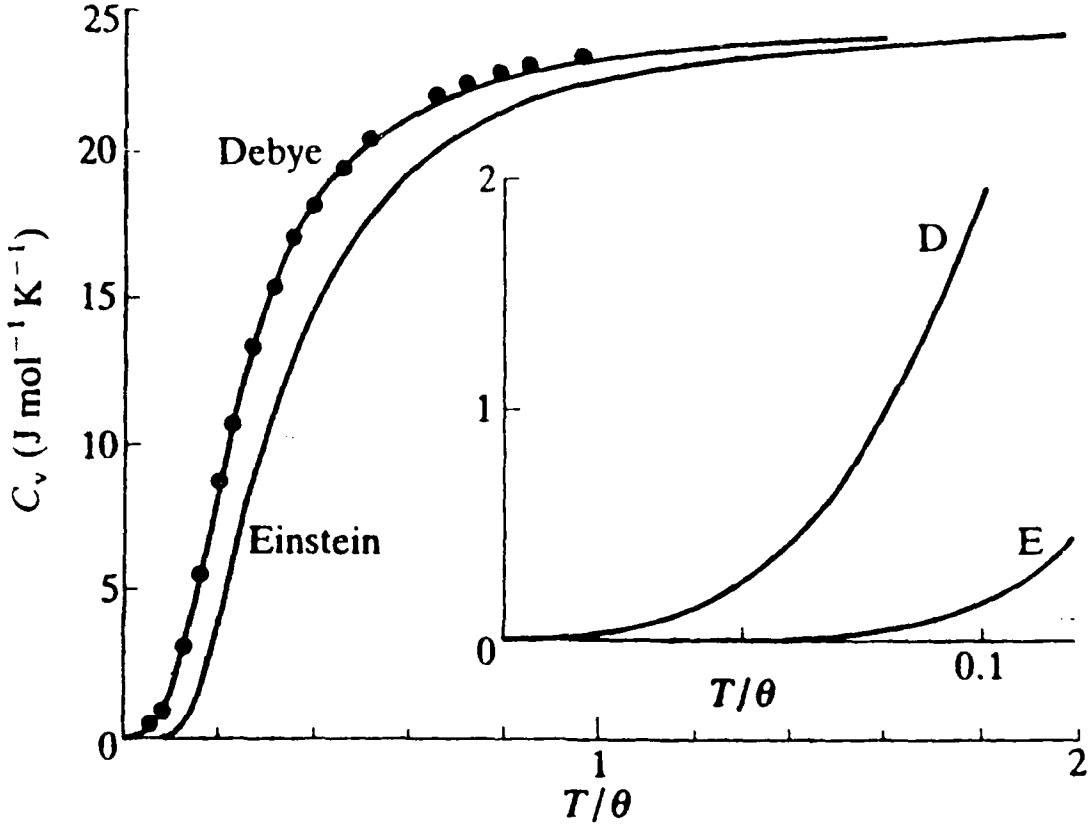

Figure. 3

The Debye and Einstein specific heat functions taken form Myers[13]. Also plotted are experimental data for silver. It can be seen that the Debye theory for the specific heat of solids does predict the correct temperature dependence for values near absolute zero.

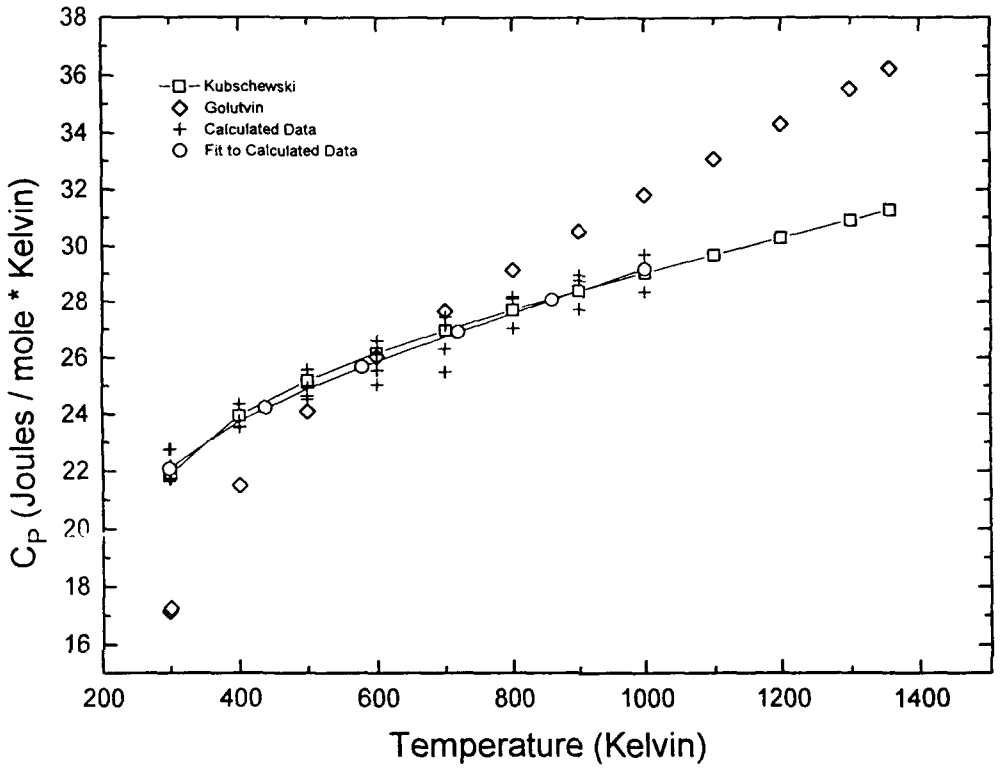

Figure. 4

The estimation of the specific heat of $TiSi_2$ by Kopp's rule. Also plotted are Golutvin's experimental data. As well as the results of Kubachewski's estimation.

To obtain this graph the C_P of $TiSi_2$ was estimated four ways: once from each of the C_P values of chromium silicide, cobalt silicide and vanadium silicide, and a fourth estimate based solely on the specific heats of Ti and Si.

A fit to these four sets of estimated values was performed to yield:

$$C_P = 21.916 + (7.4181 \times 10^{-3})T - (1.8187 \times 10^{5})T^2 + (21956 \times 10^{-8})T^2$$

The functional form of the fit is the standard form of C_P curves in the literature.

Experimental

Sample Preparation:

The first step in the experimental procedure was to produce a titanium disilicide alloy. Quantities of Ti (99.99) and Si (99.999) were massed to within ± .04% of stoichiometric $TiSi_2$. The constituents were then arc - melted in a titanium gettered argon environment (Fig. 5). Argon of 99.998 purity was flowed through the arc - melter chamber for five minutes. The flow was then sealed off, leaving the chamber over - pressured. Next a piece of titanium was melted and held in the liquid state for one minute to absorb any residual oxygen. The sample was then melted and held as a liquid for about 3 seconds.

As the samples cooled from the melt, it was apparent that they were freezing anisotropically, solidifying at the bottom first and growing into a bullet shaped ingot. This differential solidification led the samples to separate into two different phases. This separation was first suspected upon the observation that the bottom third of the sample had a different color than the rest of the sample. When the off colored part of one of the samples was x - rayed, approximately a one to one ratio of $TiSi_2$ and Ti_5Si_3 was found. X - ray analysis of the remainder of the sample showed a mixture of $TiSi_2$ and elemental silicon. In order to promote homogenization, the samples were turned on their side after solidification and remelted. The samples now solidified much more isotropically; their shape was observed to be largely spherical. X - rays of samples prepared in this manner showed single phase $TiSi_2$ (Fig. 6).

The last step in sample preparation was an anneal to relieve crystal stresses, increase homogeneity, and promote grain growth. The time and temperature for the anneal, one hour at 1300° C, were decided upon by referencing data on the annealing of aluminum and other metals.[14] This anneal was performed in a 10^{-6} torr vacuum with a tantalum getter. After the anneal, the sample was allowed to cool to room temperature by radiation; about three hours were required to cool to room temperature.

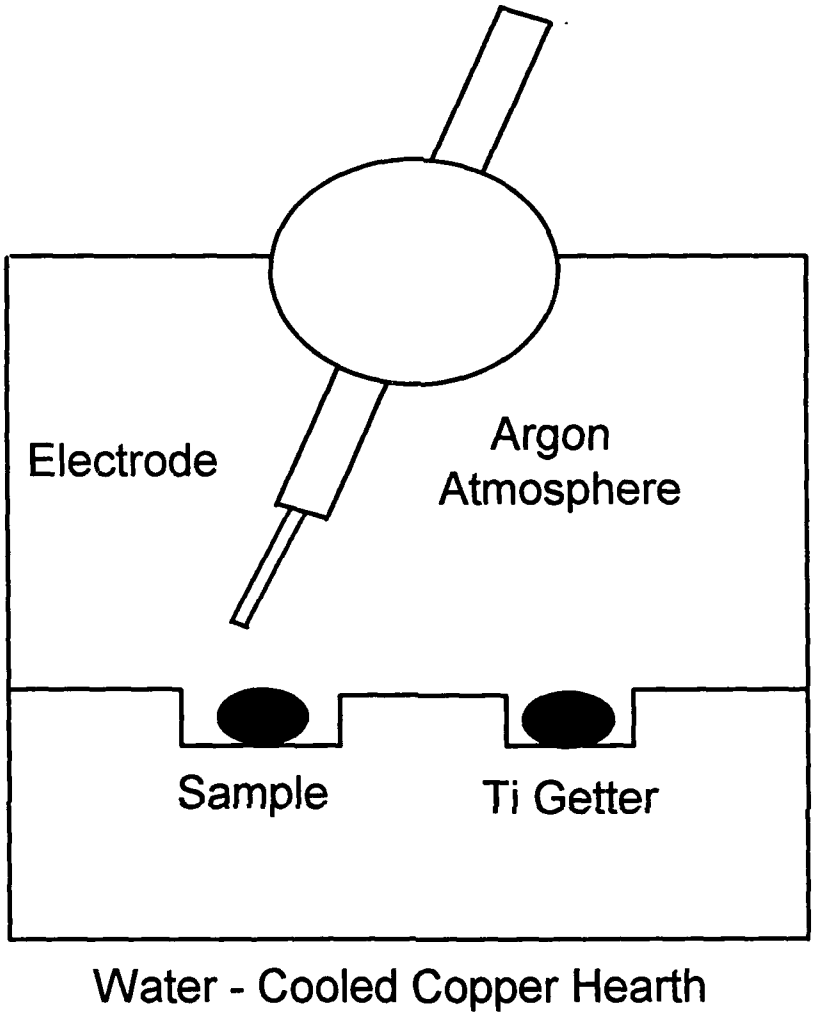

Figure. 4

A diagram of a Centorr Associates Model #5 Single Arc Arc - Melter. Both the hearth and the tungsten electrode are water cooled. The dimensions of the chamber are about 8 cm in diameter by about 7 cm high.

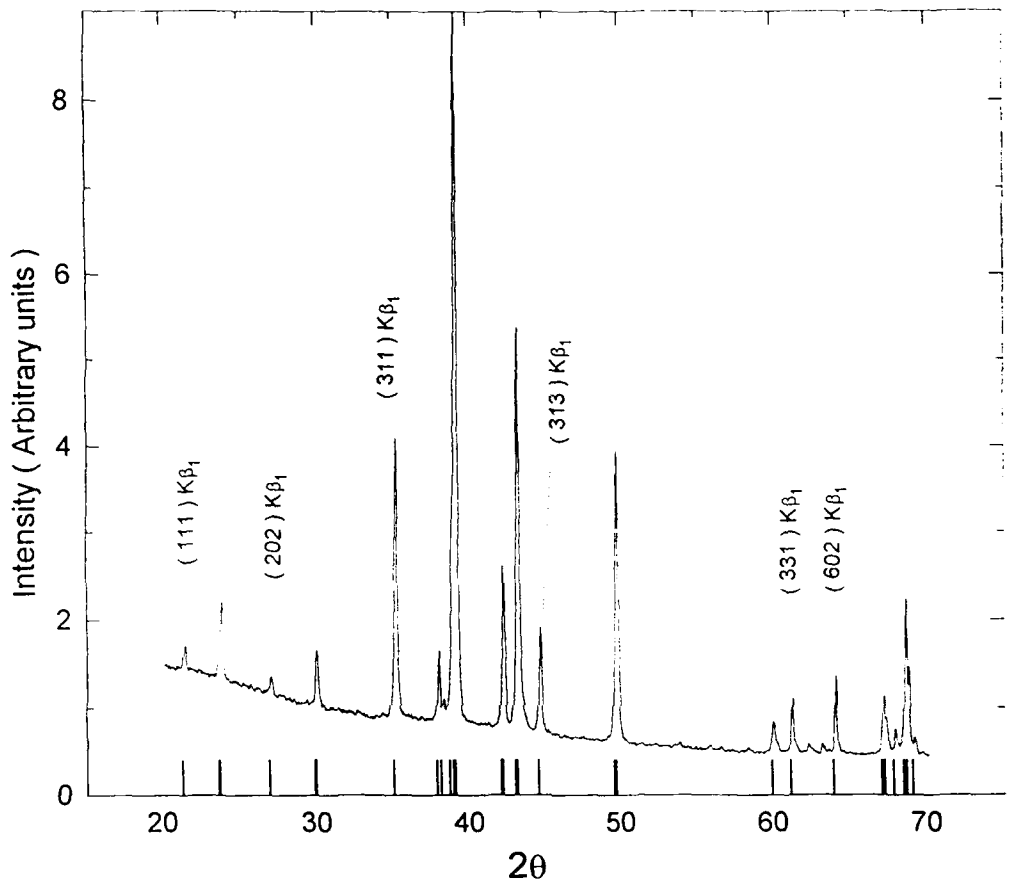

Figure. 6

A typical titanium disilicide x - ray scan. All peaks correspond to $TiSi_2$. Only those peaks used in lattice parameter refinement are labeled. The lines across the bottom of the figure are the predicted peak positions based upon the lattice parameter refined from the $K\beta_1$ peaks.

Sample Characterization:

Sample characterization was performed by means of powder X - ray diffraction and electron microprobe analysis. Specific heat measurements were made by differential scanning calorimetry.

X - ray diffraction was performed in a standard theta - two theta geometry using copper $K_{\beta 1}$ radiation. Because of the low two theta values used in this experiment the peaks of Kα doublet reflected from each plane exhibited small angular displacements from each other. This lead to difficulties in determining the exact location of each individual K_α peak. Therefore, the K_α peaks were not used in calibration or lattice parameter refinement. The background near each peak was fit to a polynomial of order three. This background was then subtracted and each K_β peak was fit to a Lorentzian curve. Both the fit of the background and the peaks were performed using curve fitting software, Peakfit.[15]

Immediately prior to the scan of the sample, a scan of a NIST silicon standard,[16] a = 5.430940 ± 0.000035 Å, was performed for use in equipment calibration (Fig. 7). The 2θ peak positions of this scan were used to estimate the systematic error in our x - ray equipment. This offset was obtained through the use of a shareware program called Cell. The program is an algorithm based on Cohen's method[17] of lattice parameter refinement. This method consists of performing a simultaneous least squares fit to all lattice parameters as a function of $\cos^2\theta$. Silicon exhibits the diamond structure, therefore the lattice parameter for the fit are calculated from the following equation[17]:

$$\sin^2\theta = \frac{\lambda^2}{4}\left(\frac{h^2+k^2+l^2}{a^2}\right), \qquad \text{Eq. 17}$$

Where a is the lattice parameter; h, k, and l are Miller indices, and λ is the wavelength of the radiation used for analysis. Because the relative systematic error in diffractometer scans are lessened as two - theta approaches 180 degrees, the y-intercept of the linear fit is

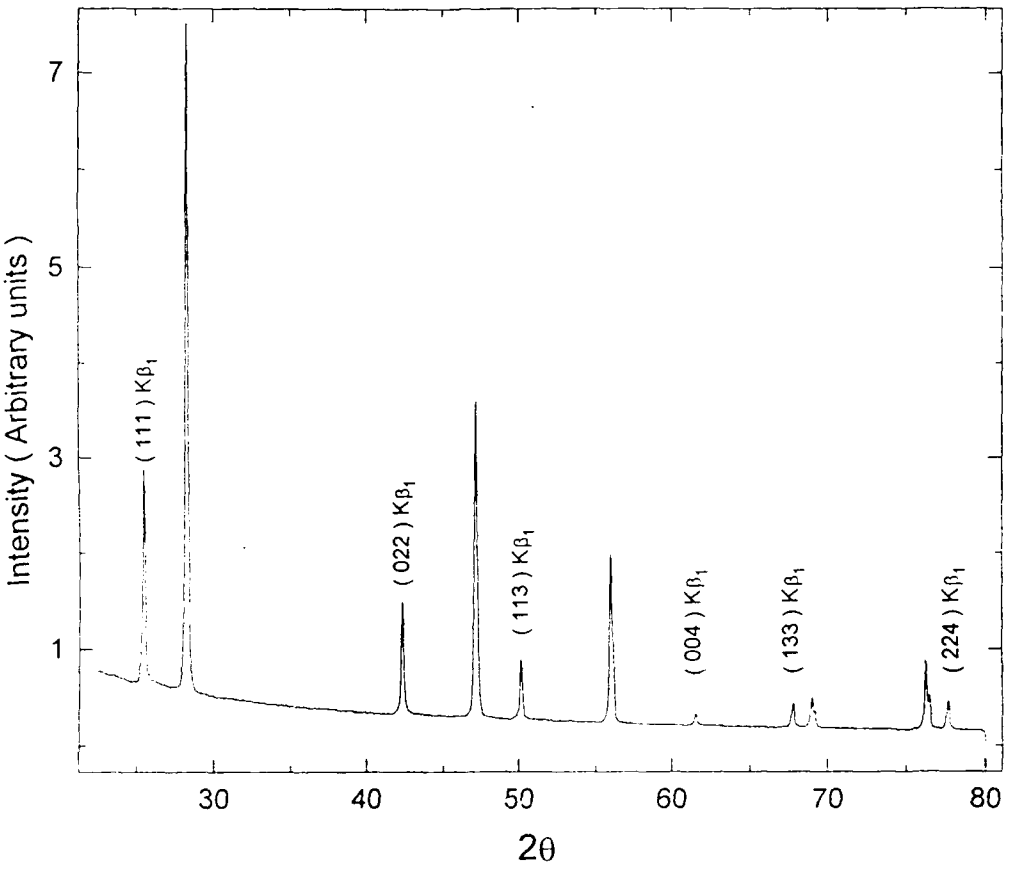

Figure. 7

An x - ray scan of powder silicon standard[18] used to calibrate the diffractometer. Unlabeled peaks correspond to the copper Kα doublet and were not used in calibration.

taken as the lattice parameter. This reduction in systematic error can be demonstrated by differentiating Bragg's law:

$$\frac{\Delta d}{d} = -cot\theta\Delta\theta. \qquad \text{Eq. 18}$$

Because $cot\theta$ approaches zero as θ approaches 90, the systematic error in the calculated lattice parameter also goes to zero. For the same reasons, the slope of the fit is proportional to the systematic error in the diffractometer.

The program, Cell, allows the user to select which parameters to vary: lattice parameter, unit cell angles, and zero point correction. Because the lattice parameters and cell angles were accurately known for the standard, these were held constant at the values supplied by NIST while the systematic error was determined. This offset was found to be 0.152 ± 0.001 two theta degrees. This value was subsequently added to the angular position of each peak obtained for the sample.

From the scan of the sample (Fig. 6) six $K\beta_1$ peaks were chosen because they were well separated from all other peaks. These six peaks were then used in the refinement of the lattice parameters for $TiSi_2$. Titanium disilicide exhibits the orthorhombic structure; the equation relating the lattice parameters and peak position for an orthorhombic structure is:

$$sin^2\theta = \frac{\lambda^2}{4}\left(\frac{h^2}{a^2} + \frac{k^2}{b^2} + \frac{l^2}{c^2}\right). \qquad \text{Eq. 19}$$

The Miller indices and 2θ for each peak are listed below, as well as a predicted 2θ calculated from the lattice parameters of Laves[18].

hkl	2θ observed	2θ calculated
111	21.52	21.49
202	27.09	27.09
311	35.24	35.21
313	44.72	44.68
331	61.33	61.28
602	64.17	64.12

Table. 1

From these six peaks the following lattice parameters were refined.

	a (Å)	b(Å)	c(Å)
Sylla et. al.	8.2607 ± 0.0004	4.7967 ± 0.0003	8.545 ± 0.002
Laves[18]	8.252 ± 0.006	4.783 ± 0.004	8.540 ± 0.006
Jeitschko[19]	8.2671 ± 0.0009	4.8000 ± 0.0005	8.5505 ± 0.0011

Table 2.

Our parameters show good agreement with the literature values, falling between the values reported by Laves and Jeitschko in each case.

As a second check of sample characteristics, electron microprobe in the wavelength dispersive mode was performed. In electron microprobe, the sample is bombarded with electrons, stimulating the emission of x - rays. These x - rays will have the characteristic frequencies of the elements in the sample. By counting the number of x - rays emitted at each wavelength, the composition of the sample can be determined.

A back - scatter electron image of the $TiSi_2$ sample is presented in Fig. 8. Analysis by electron microprobe in the wavelength dispersive mode indicated that, over a region with a length scale of approximately 400 μm, the sample was homogeneous to within approximately 1%. Variations of this length scale are at the lower resolution limit of the instrument; surface roughness can have a profound influence on signal strength at this scale. The overall stoichiometry of the sample was found to be $TiSi_2$, though the error in stoichiometry determination by this technique can be as much as 5% or 10%.

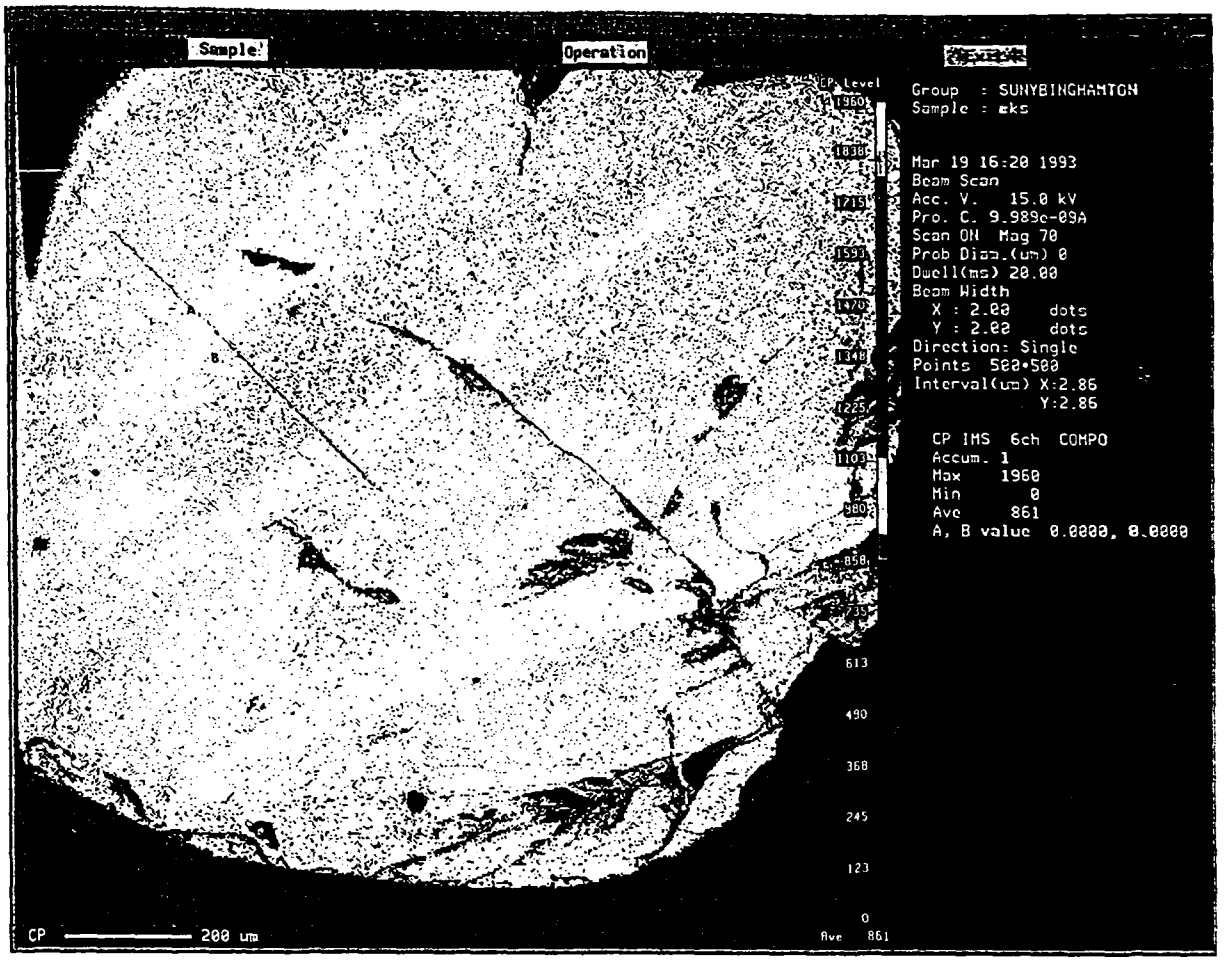

Figure. 8

A back - scatter electron image of a fraction of the sample. The variations in gray scale could be actual inhomogeneities in the sample or they may be solely due to surface effects. Wavelength dispersive electron micro - probe has shown variations corresponding to the color change. It should be noted however, that we are working at the resolution edge of the instrument and these variations could be due solely to the machine.

The specific heat measurements of $TiSi_2$ were made by differential scanning calorimetry, DSC. Before the actual measurements and results are presented an overview of the general operating principles of a DSC and the procedures that were followed to measure the specific heat of $TiSi_2$ will be discussed.

The differential scanning calorimeters used in this experiment were manufactured by Perkin Elmer. A Perkin Elmer DSC - 2 modified for liquid nitrogen temperature measurements was used to collect data from 100 to 340 K. From 303 to 500 K a Perkin Elmer DSC - 4, cooled by an ice bath, was used for data collection. Both of the DSC's were interfaced to micro - computers for data acquisition and analysis.

The basic design of a differential scanning calorimeter is shown in Fig. 9. There are two calorimeters in each DSC. Each calorimeter consists a platinum cup and cover, a heater and thermometer. The calorimeters are encased in an aluminum block. This entire assembly is referred to a DSC head. The space between the calorimeters and aluminum block is purged with a controlled flow of argon or helium gas. To make a specific heat measurement a sample encased in an aluminum pan is placed in the left calorimeter; the right calorimeter is left empty as a reference. In an ideal DSC, the sample calorimeter and reference calorimeter would be exact duplicates.

To acquire data the DSC is programmed to heat the sample calorimeter and the reference calorimeter at the same specified rate. Due to the heat capacity of the sample, the sample and its calorimeter will have a tendency to lag the reference calorimeter in temperature as the DSC is heating. Circuitry inside the DSC is designed to compensate for this temperature lag by supplying more power to the heater of the lagging calorimeter, keeping the difference in temperature between the two thermometers zero as the temperature is raised. The power required to keep this difference in temperature zero is converted to a proportional number of volts. This is the output signal of the DSC.

As the DSC is heating, the power supplied to each heater in the DSC flows into several different heat sinks. For the sample calorimeter, the sample itself is only one of

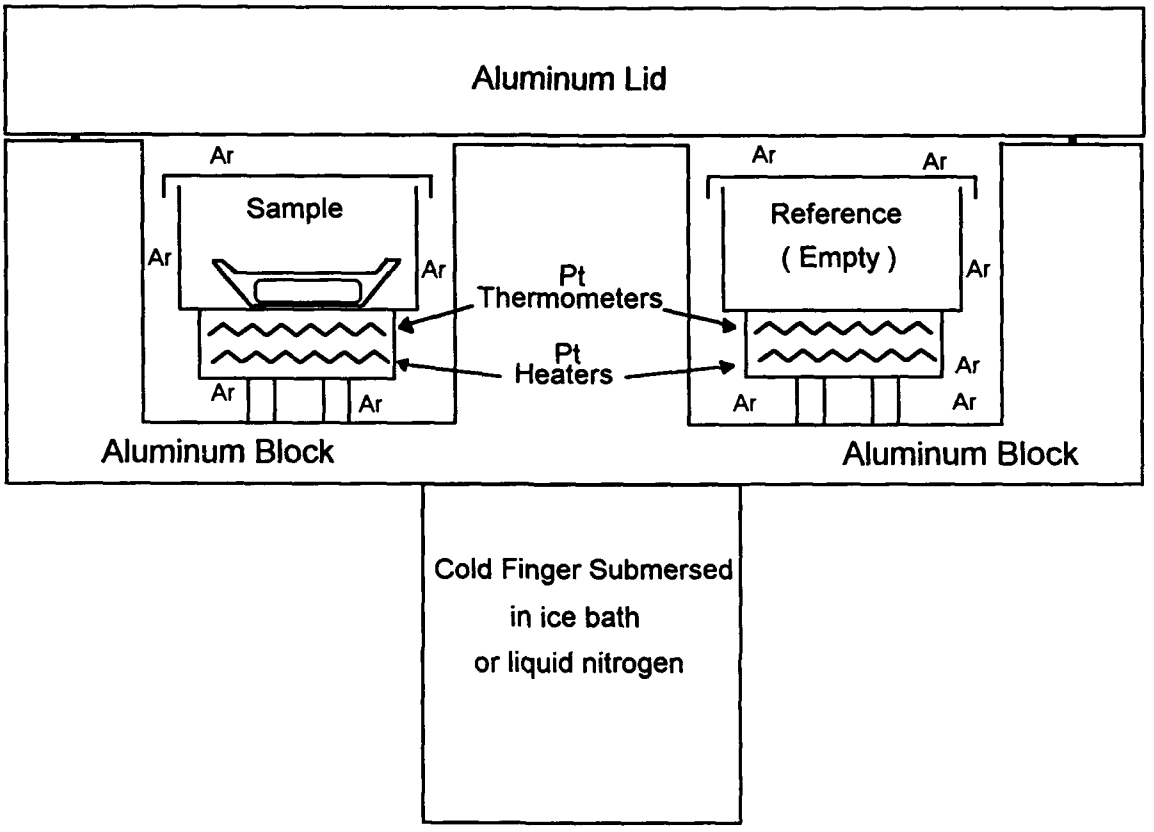

Figure 9.

Simplified schematic of a Differential Scanning Calorimeter. The entire block and head assembly is contained in a glove box over - pressured with nitrogen gas. Both the sample calorimeter and reference calorimeter of the DSC - 4 are purged with a controlled flow of argon gas. Helium was used as the purge gas for the DSC - 2. An "O" ring is used to make a gas tight seal between the lid and block of the DSC - 4.

these heat sinks. This is due to the sample's inherent heat capacity. Another sink is the aluminum pan in which the sample is encapsulated, due to its inherent heat capacity. All other heat sinks: the DSC cup, the cold finger, radiative losses, etc.; can be grouped together as *other*. The heat flow into the sample calorimeter can now be written as:

$$\frac{dq_s}{dt} = C_{P_{sam}}\frac{dT}{dt} + C_{P_{pan}}\frac{dT}{dt} + other_{sam}. \qquad \text{Eq. 20}$$

The $other_{sam}$ term in Eq. 20 is of course dependent upon temperature, sample placement and shape, as well as other factors.[20]

Because the reference calorimeter is left empty, its only heat loads are such things as the cold finger, the DSC cup, etc., therefore the heat flow into this calorimeter will be:

$$\frac{dq_r}{dt} = other_{ref}. \qquad \text{Eq. 21}$$

The signal output from a DSC is proportional to the difference in heat flow between the two sides. The difference in heat flow between the two calorimeters is mathematically the difference of Eqs. 17 and 18:

$$\frac{dq_s}{dt} - \frac{dq_r}{dt} = C_{P_{sam}}\frac{dT}{dt} + C_{P_{pan}}\frac{dT}{dt} + baseline.$$

$$\equiv F \cdot signal \qquad \text{Eq. 22}$$

This difference in heat flows is related to the output signal of the DSC by a proportionality constant. The constant is F, the calibration constant of the DSC. In the above equation the *baseline* term denotes the difference in the heat flow to the *other* heat sinks, $other_{sam} - other_{ref}$. If both sides of the DSC were left empty, the signal would only depend solely upon the quantity $other_{sam} - other_{ref}$. This is the baseline signal of the DSC. This value is non-zero because the *other* heat losses of the two calorimeters are not completely identical. From Eq. 22 it can be seen that this signal will exist even for zero heating rate. The baseline does however depend upon the temperature of the calorimeters (Fig. 10).

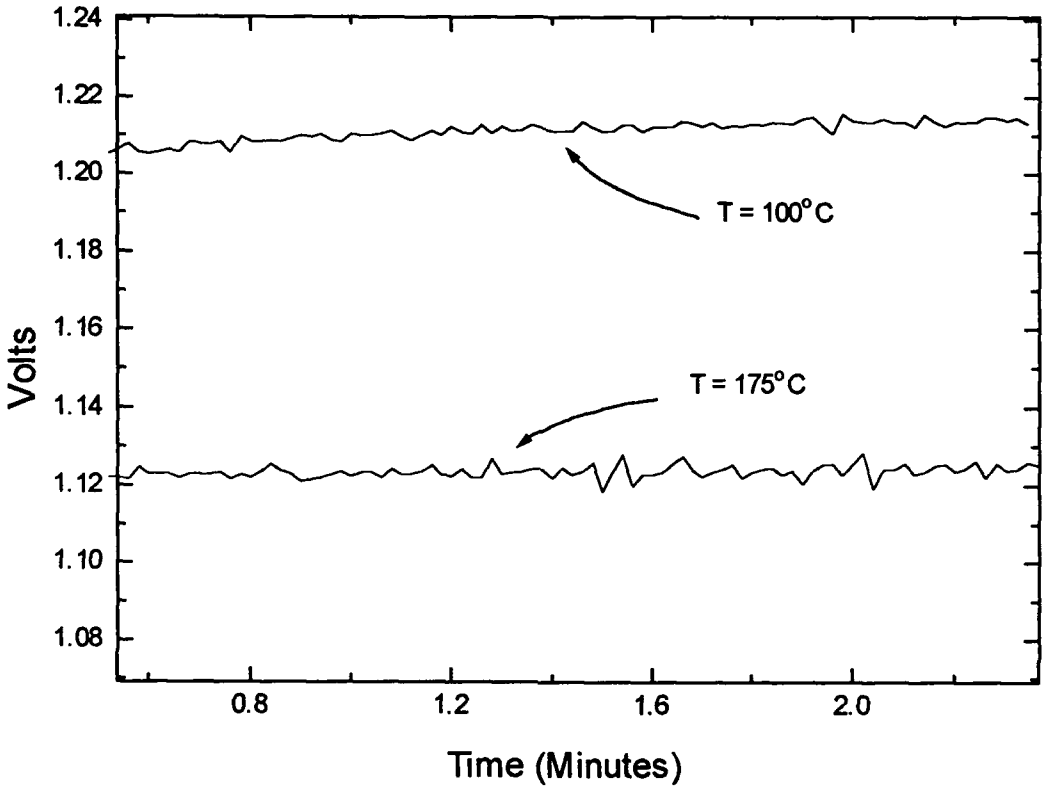

Figure. 10

Two isothermal baselines. Note that while isothermal signal is dependent upon temperature, the signal does not necessarily increase with temperature. In order to evaluate specific heat data, the offset due to the isotherm must be subtracted away.

The problem now is to extract the desired quantity, $C_{P_{sam}}$, from the signal defined by Eq. 22. The last two terms must be subtracted from Eq. 22 and the calibration constant, F must be determined.

To accomplish this, DSC signals other than the actual $TiSi_2$ signal are required. A signal for an empty pan is required to subtract the contribution to the signal from the pan in which the sample was encapsulated. If performed correctly, this subtraction will also account for the baseline component of the signal. The signal generated by a DSC for an empty pan is:

$$F \cdot signal_{empty} = C_{P_{pan}} \frac{dT}{dt} + baseline_{empty}. \qquad \text{Eq. 23}$$

Subtraction of this equation from Eq. 22 yields:

$$F \cdot \left[signal_{sam} - signal_{empty}\right] = C_{P_{sam}} \frac{dT}{dt} + baseline_{sam} - baseline_{empty} \qquad \text{Eq. 24}$$

The baseline component of the sample and empty signals are not necessarily equal. But if all signals are mathematically compensated to the same baseline before the empty pan subtraction, the baseline terms will cancel and Eq. 45 becomes:

$$F \cdot \left[signal_{sam} - signal_{empty}\right] = C_P \frac{dT}{dt}. \qquad \text{Eq. 25}$$

Since the heating rate is known, all that remains before the value of C_P can be found from Eq. 25 is to determine F, the calibration constant of the DSC. This can be found by acquiring a signal for a sample of known specific heat. Before the details of this calibration and just how the signals are compensated to the same baseline are discussed, the experimental procedure used for the measurement of $TiSi_2$ will be presented.

Before this discussion is begun, the use of the word "sample" should be defined. In the following paragraphs the word "sample" is used generically for whatever is in the left calorimeter of the DSC e. g. an empty pan sample, or a $TiSi_2$ sample.

A typical DSC "scan" for any sample began with a three minute isotherm at the low end of the temperature range. Then the sample was heated at twenty Kelvin per minute for seventy - five degrees. The temperature of the sample was then held at the high end of the temperature range for an isotherm of nine minutes. A plot of a typical temperature profile, as well as the signal of a typical scan, are shown in Fig. 11. Data on the isotherms before

and after each heating range were acquired because they are required for data analysis, as will soon become apparent.

Each sample was scanned three times before preceding to the next sample. The first scan was performed to allow the sample to equilibrate with its surroundings. The third run was used for data analysis. The second run was used to check the stability of the DSC by subtracting run two from three.

To measure the specific heat for any given temperature range, an empty pan was scanned first. This signal was acquired in order to be subtracted from the other sample signals as described above. Next a specimen of known specific heat, copper, was scanned. This signal was used in calibration. Then scans of up to three samples of $TiSi_2$ were performed. And lastly a, second specimen of known specific heat, molybdenum, was scanned. The scan of this sample was used to estimate the error in the measurements. A typical set of four scans is shown in Fig. 12.

Variations in isothermal baselines can be seen in Fig. 12. The temperature dependence of the baseline, as previously discussed, is present; i. e. the baselines for the initial and final isotherm of each scan are different because they are at different temperatures (Ref. again Fig. 10). It is also observed that, for the same temperature, the baselines from scan to scan are different. From Eq. 22 it can be seen that these variations should not depend on the heat capacities of the various samples because the heating rate is zero on the isotherms. Therefore these differences are most likely due to long term drift in the DSC itself or any slight differences in pan placement or shape.

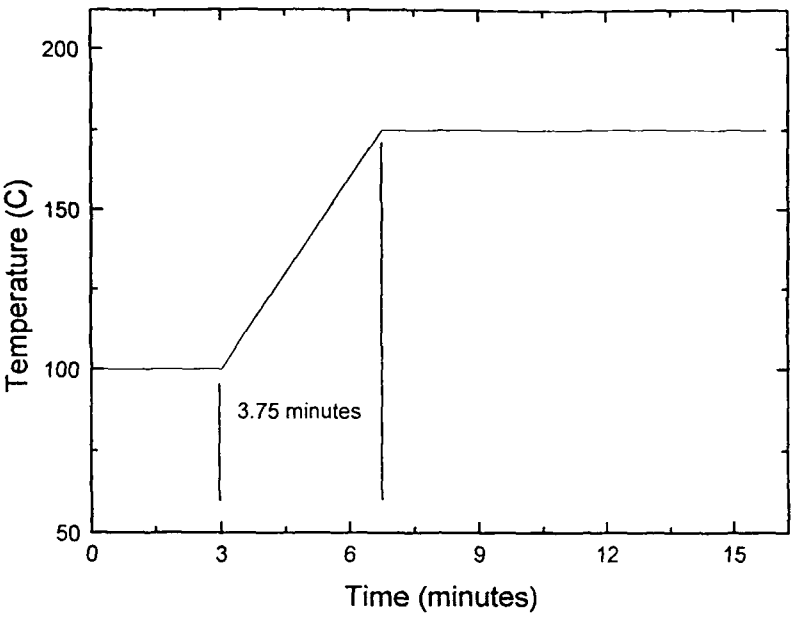

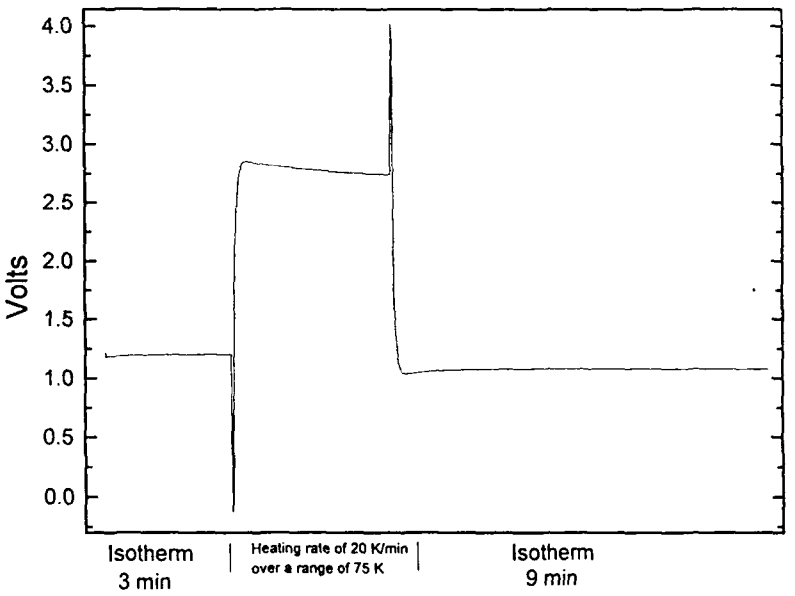

Figure. 11

A typical temperature profile and typical DSC signal.

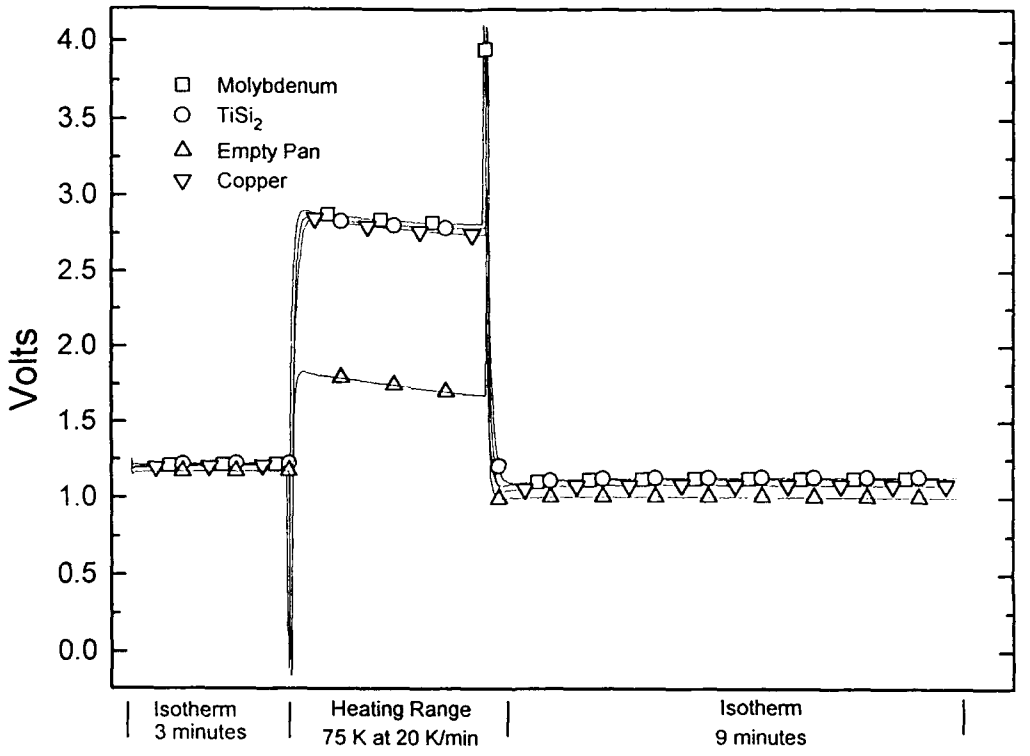

Figure. 12

The raw signals of the scans required to measure specific heat by DSC. Notice that the isothermal baseline is not the same before and after the heating of the samples. Also note the baselines for each signal are different.

The first step in obtaining the specific heat of $TiSi_2$ from the scans shown in Fig. 12 is to account for these variations in baseline by adjusting the signals so their baselines all have the same value. This will allow the *baseline* terms is Eq. 22 to cancel. The problem is that the exact form of the baseline during the heating range is unknown. An assumption is made that if the isothermal baselines of all the signals are equal, then the baselines of the signals during the heating range are also equal.

To apply this assumption to the isotherms of each signal the isotherms are fit linearly. This fit for each isotherm is then subtracted to give all isotherms the same value, zero. To apply this assumption to the heating range of each signal, the final isotherm must first be extrapolated back through the transients to the end of the heating range (Fig. 13). A linear interpolation is then performed from the end of to the initial isotherm to the beginning of the final isotherm (Fig. 14). This line is subsequently subtracted from the signal (Fig. 15). Although this line is not indicative of the actual baseline during the heating range, its subtraction largely accounts for any variation in baseline from run to run. The baselines should now be equal and will cancel with the empty pan subtraction.

To give the reader some idea of what the actual baseline for the heating range may look like, a typical scan was performed with both calorimeters empty (Fig. 16). Although not completely indicative of the actual baseline, it is shown to demonstrate that the baseline is <u>not</u> a linear interpolation between the isothermal baselines.

The signal from the empty pan scan is now subtracted from the signals of the other scans. This subtraction accounts for the contribution to the signals due to the pans in which the samples are encapsulated. It also subtracts out the baseline contribution to the signal since now the baselines are theoretically all equal (Fig. 17). All that remains now is to determine the calibration factor of the DSC, F, in Eq. 25.

Since the specific heat values for copper found in the literature are well accepted,[21,22] the copper sample heat capacity run can be used to find the calibration factor, F. These values are those compiled by Furukawa et. al. in 1968.[23] The reported

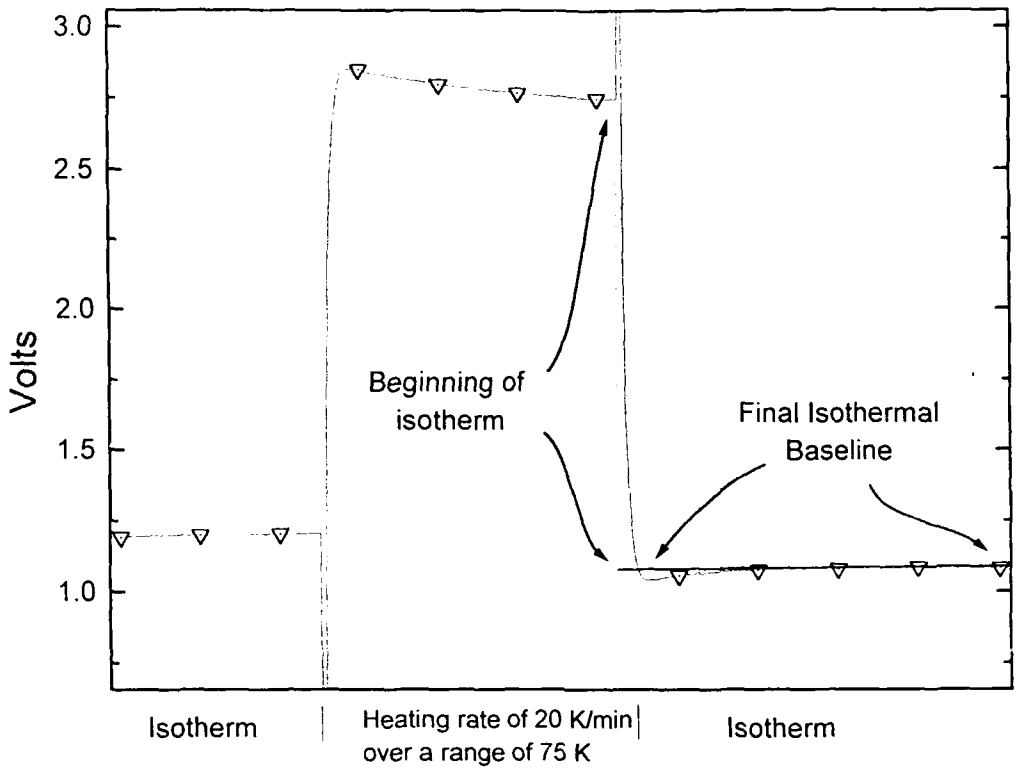

Figure. 13

A typical run having its isothermal baselines corrected to the same common value. The final isotherm has been extrapolated back to the end of the heating range. The next step will be to interpolate a baseline between this extrapolated point and the end of the initial isotherm.

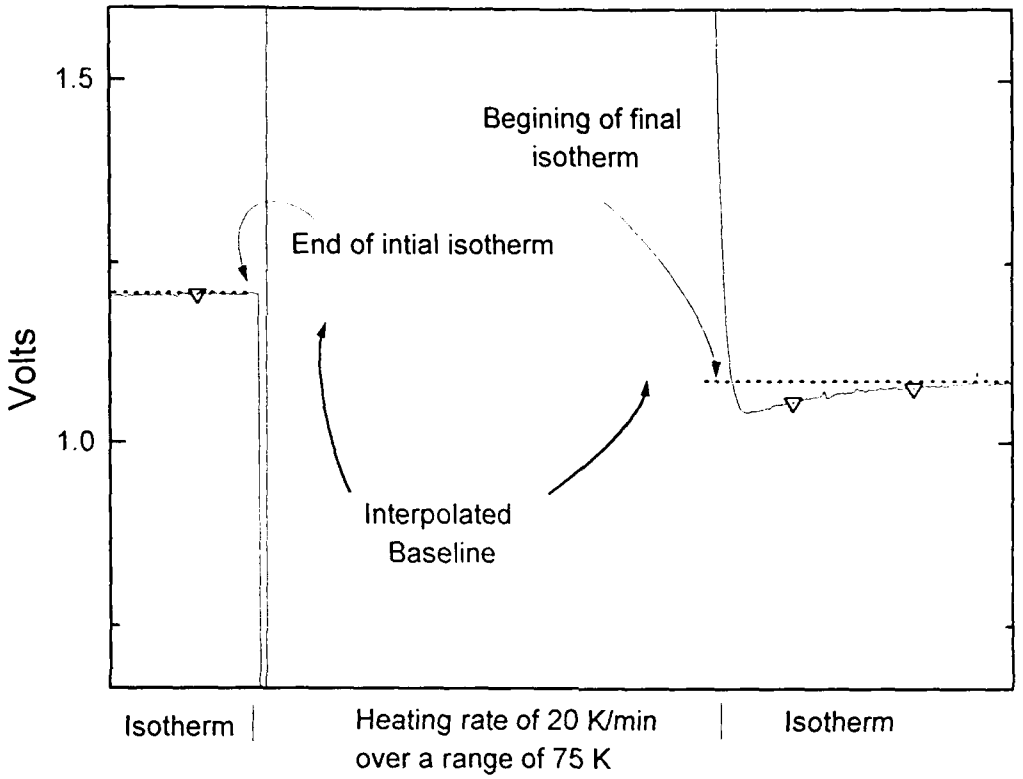

Figure. 14

An expanded view of the previous figure being corrected to a zero baseline. The final isotherm has been extrapolated back to the end of the heating range. A line was then interpolated between the points where the heating begins and ends. This line will now be subtracted from the signal to give its true "displacement" in Volts.

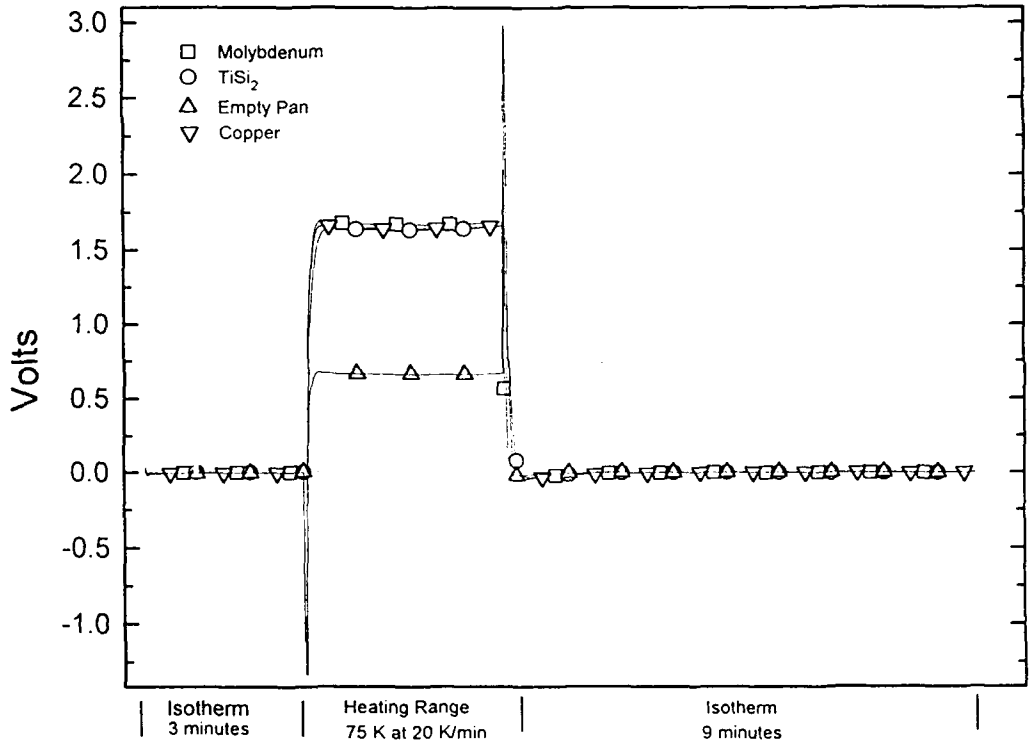

Figure. 15

A typical set of signals after being compensated for variations in baseline. The height of each signal above the zero line is should now be proportional to it heat capacity. For the samples this still includes the part of the signal due to their pans. The empty pan run can now be subtracted from the rest of the runs.

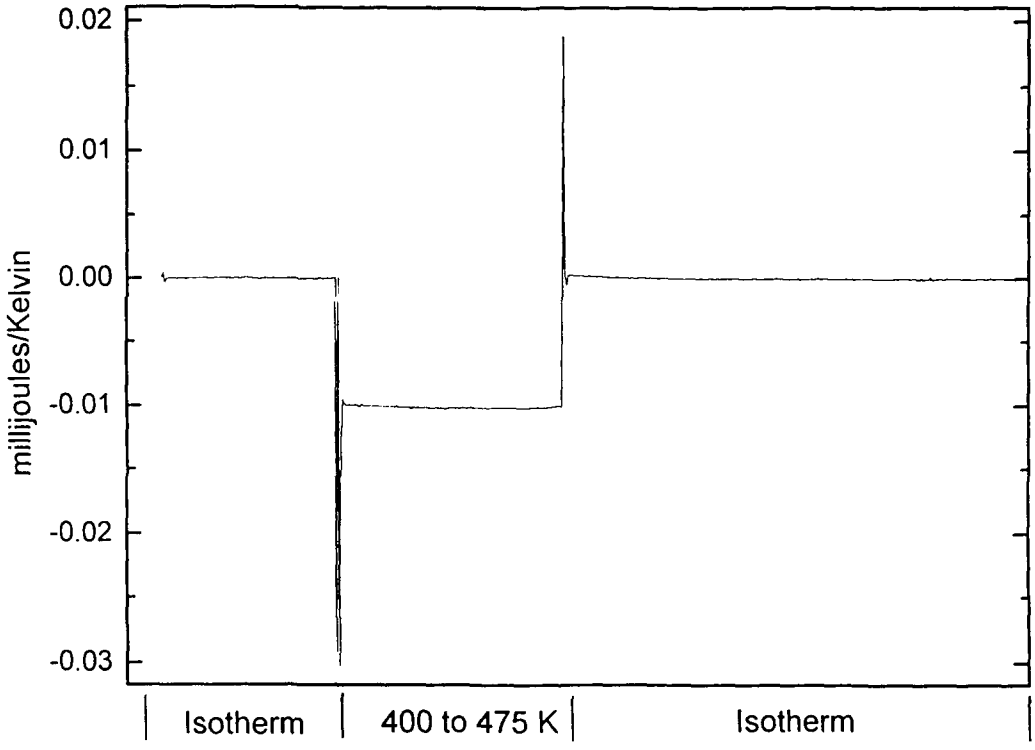

Figure. 16

The difference in heat flow to the two cup assemblies for a typical scanning range. Both cups are left empty but otherwise all other factors are the same as those for the runs to measure heat capacity. The output signal was converted to millijoules/Kelvin by multiplying by the calibration factor determined for a set of heat capacity scans from the same day. The negative amplitude signifies more heat flowing to the reference side than the sample side. The plot is presented to show that the baseline for the heating range is not a linear interpolation between the isothermal baselines.

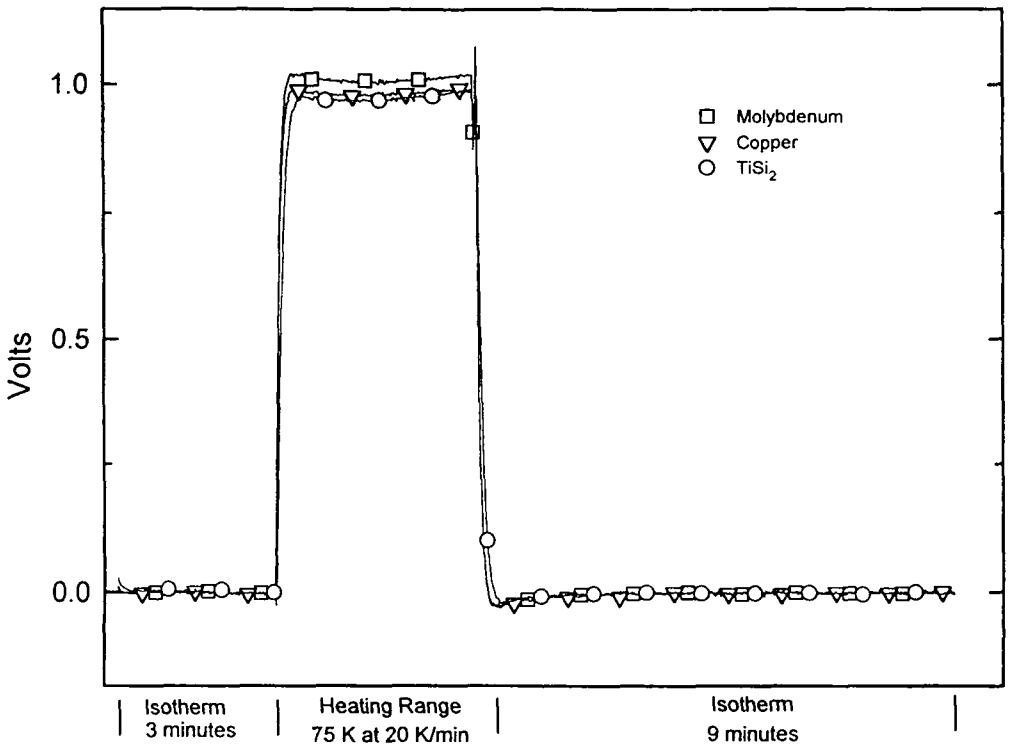

Figure. 17

Signals after having the empty pan run subtracted. The signals should now be proportional to the heat capacity of the samples themselves. The copper signal can now be used to determine the calibration of the DSC.

uncertainties in these values for the range of 100 to 300 K is less than .3%. A plot of the reported error in these data is contained in Appendix 1.

After the copper signal has had the empty pan run subtracted, it is divided by the number of moles in the copper sample. The literature values for the specific heat of copper are now substituted into Eq. 25 to yield:

$$F = \frac{C_{P_{Literature}} \, dT/dt}{signal_{copper} - signal_{empty}} \cdot moles\ of\ copper \qquad \text{Eq. 26}$$

The calibration factor, F, has the units of $Joules / Volt \cdot s$.

The $TiSi_2$ and molybdenum signals are then each individually multiplied by this calibration factor. The values obtained are the heat capacities of these samples. These values are then divided by the respective number of moles in each sample to obtain their respective specific heats,

$$C_{P_{sample}} = \frac{F \cdot \left(signal_{sample} - signal_{empty}\right)}{moles\ of\ sample \cdot dT/dt}. \qquad \text{Eq. 27}$$

The measured value of the molybdenum specific heat is then compared to its literature value[24,25,26] to estimate the error in each set of measurements. The values are taken form Desai's evaluation. Desai reports errors for this data from ± 1.5% to ± 3%. A graph of the reported error in these values is contained in Appendix 3. To improve accuracy and increase precision, as well as save time, an algorithm[27] to perform the above procedures has been written in Asyst.[28]

Factors Affecting the Accuracy of DSC Measurements:

Although it has been shown that measurements of specific heat by differential scanning calorimetry are capable of producing results with ±1% accuracy,[29] there are many sources of error that must be minimized before this level of accuracy can be attained. Many authors give lists of factors that may adversely affect DSC specific heat

measurements. There has, however, been little attention paid to the relative magnitudes of the errors caused by these various sources. Due to this lack of quantification, procedures for the minimization of error in DSC measurements seem to be rooted mostly in superstition and myth.

Therefore, in this paper an effort will be made to not only explain the procedures used to minimize the errors in the measurements; but also, whenever possible, the quantitative effects that these procedures have had in the overall error in these measurements will be discussed.

Calibration:

Before accurate specific heat measurements can be made, a compensation must be made for the inherent thermal lag of a DSC. This correction is necessary because the sample temperature tends to lag the temperature reported by its thermometer. This lag is due to the heat capacity of the sample and the thermal resistance between the sample and the thermometer. This lag has been characterized by Patt et. al.[20] as:

$$\Delta T = \beta(\tau_x + R_0 C_S) + \Delta T_C, \qquad \text{Eq. 28}$$

where β is the heating rate, ΔT_C is a constant offset, τ_x is a time constant of the instrument, R_0 is the thermal resistance between the thermometer and sample, and C_s is the heat capacity of the sample and pan. Without compensation for this lag, an otherwise accurate measurement of C_P will be assigned to an incorrect temperature.

Although this generally does not constitute a significant error, we attempt to minimize any such error as much as possible. The error caused by thermal lag can be compensated for by determining ΔT in Eq. 28. This is accomplished by heating selected materials of high purity through known transition temperatures. The difference between the displayed transition temperature and the accepted transition temperature is ΔT (Figs. 18, 19) For the most accurate results ΔT should be found near both ends of the temperature range in question, and preferably at points in between.

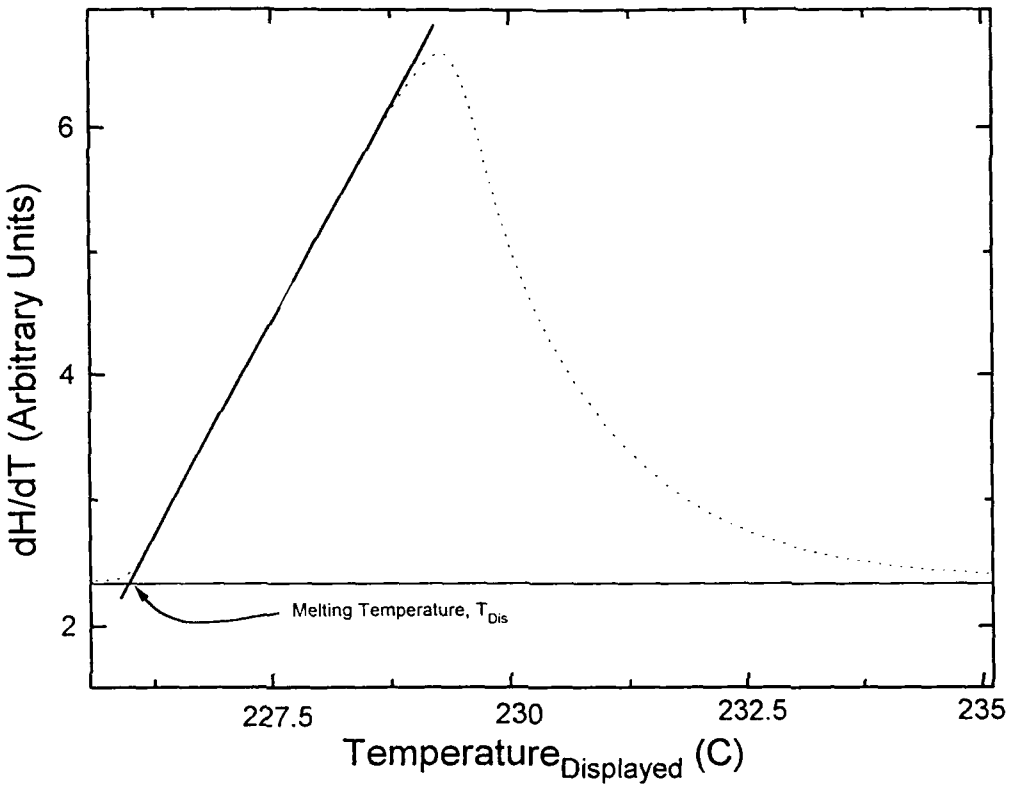

Figure. 18

A DSC signal depicting the melting of Sn. The DSC has been programmed to heat at twenty degrees per minute, the same scanning rate used for specific heat measurements. The leading edge of the signal is extrapolated to where it intersects the baseline.

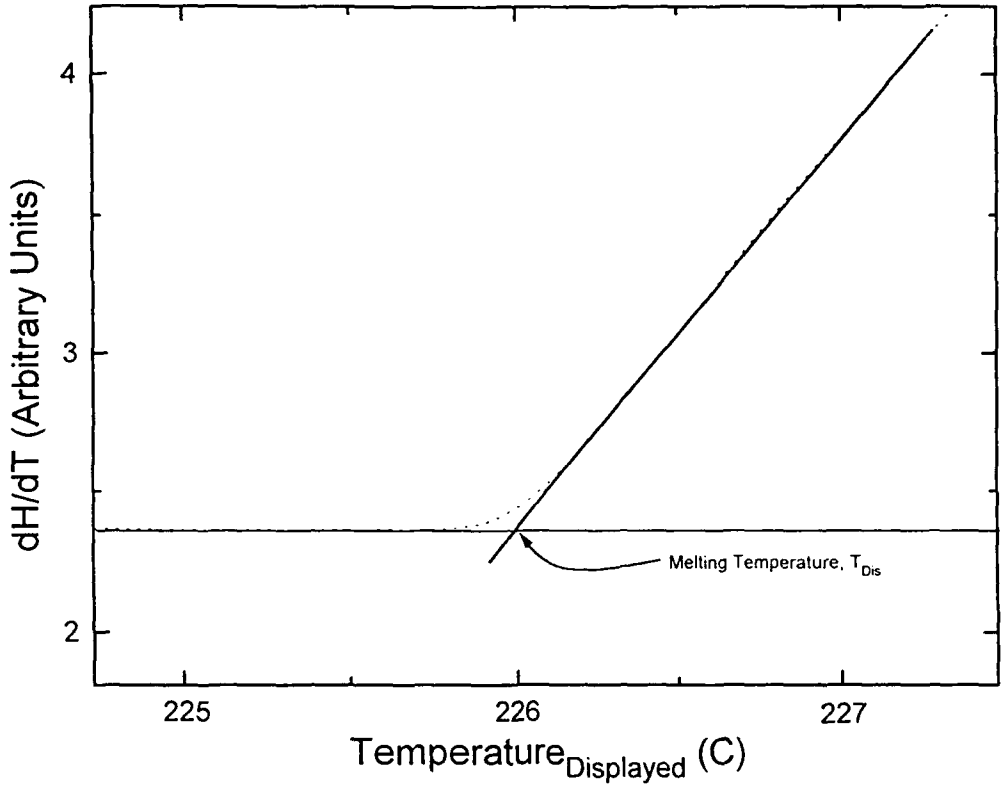

Figure. 19

The leading edge of the signal is extrapolated to where it intersects the baseline. The intersection is the displayed melting point of Sn. This value is then subtracted from the actual melting point to yield the temperature lag of the DSC.

In order for this correction to be the most effective, β, τ_x, R_0, C_S, and ΔT_c for the specific heat runs should be allowed to vary as little as possible from their values for the calibration run. The primary concern is due to the quantities R_0 and C_S. The heating rate for data acquisition was always twenty Kelvin per minute. The quantity τ_x is a constant of the machine and has been proven to have long term stability.[19] The constant offset, ΔT_c, in Eq. 28 is mostly a characteristic of the instrument and is very stable, but this offset will exhibit small variations with changing R_0 and extreme changes in pan shape.[20]

The calibration of the DSC - 2 was performed using the melting point of mercury at 234.28 K, a crystal transition in cyclopentane at 122.1 K, a crystal transition in cyclohexane at 138.1 K, and the melting point of cyclohexane at 279.7 K.[30] This calibration was performed in the spring of 1990. Although DSC instruments have shown long range stability, the accuracy of this calibration should now be questioned. The reason the DSC - 2 was not re-calibrated is the non - availability of calibrants, specifically cyclopentane.

The calibration of the DSC - 4 was performed April 1993, using In (4N), Sn (4N), and Pb (4N). A plot of this calibration is contained in Fig. 20. An effort was made to match the total heat capacities of the calibrants and the heat capacity samples. Although the heat capacity of the calibrant samples was not perfectly matched to the heat capacity samples, the difference in thermal lag caused by this variation has been estimated to be within ± 0.1 K, through the use of Eq. 28 and the Dulong Petit value of C_P.

Thermal Contacts:

The thermal contacts between the sample and the DSC cup are also important factors to be considered. From Eq. 28 it can be seen that the difference in temperature between the thermometer and the sample is directly related to the thermal resistance between them. This resistance is composed of five components: 1.) the resistance between the thermometer and the bottom of the DSC cup, 2.) the resistance at the interface of the DSC cup and sample pan, 3.) the resistance through the wall of the pan,

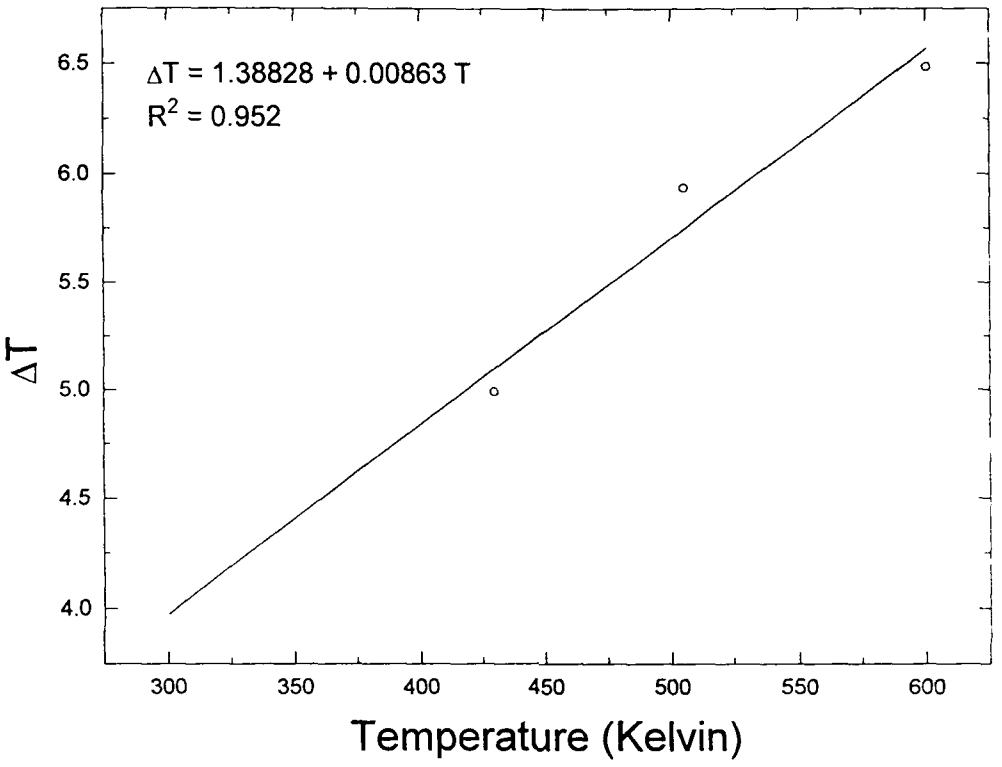

Figure. 20

A calibration plot for the DSC - 4. The error in the data is on the order of the point size. The fit of the data is extended to show the entire range of specific heat measurements. Three different metals were used in calibration: indium (4N), melting point of 429.76 K; tin (4N), melting point of 505.06 K; lead (4N), melting point of 600.6 K.

4.) the resistance at the interface of the sample and the pan, and finally 5.) the internal resistance of the sample (Fig. 21). Any temperature lag caused by these resistances, excluding the sample's internal resistance, can be corrected by the calibration previously discussed (Eq. 28) provided these resistances remain the same as those of the calibration run. In other words, the pan bottoms should all have roughly the same shape. Since all pans are very close in thickness, resistance three will not vary significantly. Neither will the resistance of the DSC cup; as it is an integral part of the equipment and very stable. The remaining resistances can vary, and the factors affecting them should be closely monitored. Also, by attempting to minimize the magnitudes of these resistances, any variations from pan to pan will cause a smaller difference in temperature lag.

The resistance between the DSC cup and sample pan is a function of the roundness of the bottom of the pan. The rounder the pan bottom, the poorer the thermal contact; hence, a larger resistance. Therefore, it is important to keep the bottoms of all pans as flat as possible. This will keep the total resistance low. Flat is also a well defined shape, and deviations from this shape will be easier to detect.

To minimize the internal resistance in the sample and the resistance between sample and pan, samples of a solid disk geometry tightly pressed to the pan should be used. To keep the sample in good contact with the pan, two pan bottoms (Perkin - Elmer part#0219 - 0062) can be used. If the sample is not available in disk form, a fine powder is preferable to larger pieces. A powder sample should have a lower over-all thermal resistance because of the higher packing fraction obtainable. Also, it is possible to obtain greater thermal contact with the pan because more sample can be packed tighter while maintaining the flatness of the pan bottom. It should be noted that because the errors caused by internal resistances in the sample cannot be corrected by Eq. 28, it is of paramount importance to keep the internal resistance of the sample to a minimum.

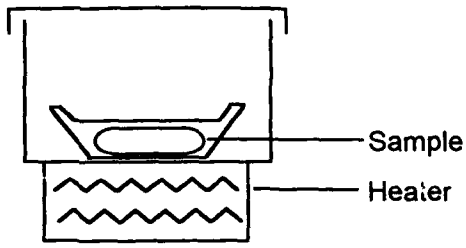

5	Resistance in the sample
4	Resistance between sample and pan
3	Resistance due to pan material
2	Resistance between pan and DSC cup
1	Resistance due to DSC cup material
	Thermometer

Figure 21.

Schematic representation of the resistances between the thermometer and the sample. The resistance due to the pan material and the resistance due to the DSC cup material are constant. The remainder of the resistances can vary and any factor that may affect these values need to be carefully monitored.

Heat Losses due to Pan Shape:

Another way in which specific heat measurements can be corrupted is through a variation in overall pan shape. Differently shaped pans will experience differences in heat loss due to radiative and convective effects.[20] We expect that these effects will become more prevalent at higher temperatures due to the T^4 nature of radiative losses. To minimize this error, all pans should have the same shape and extreme care should be taken not to bend the sides of the pans when handling them with tweezers.

Based on the these considerations each substance was hermetically sealed between two aluminum pan bottoms in an argon atmosphere at a pressure of approximately 75 torr. The Cu (50mg) and Mo (80mg) samples were in the shape of solid disks of roughly the same diameter as the pan bottom. The $TiSi_2$ (30mg) sample was ground to a fine powder. The samples were sealed in an argon atmosphere to minimize the effects of oxidation.

The reason the materials were sealed in a 75 torr atmosphere was to keep the pans from deforming at higher temperatures due to gas expansion. For pans sealed in approximately an atmosphere of argon, we have experienced difficulties in obtaining accurate specific heat data in the 500 to 800 K range. It is believed that deformation of the pans may be a large part of the problem.

The increased thermal resistance between the pan and DSC cup and the increased resistance between the pan and sample caused by pan expansion has been investigated. Plots of the signals obtained for copper and molybdenum samples before and after pan expansion (Figs. 22 and 23) demonstrate this increase. The time constants, *RoCs*, can be obtained from exponential fits to the data of Fig. 23. The difference in thermal lag between the two runs can then be calculated from Eq. 28. The difference in lag has been found to be about to be about 2 K. This difference in temperature can not account for the amount of error we have experienced at high temperatures. It should be noted, however, for temperatures in the 100 K range where there is a large dC_P/dT, this same difference in

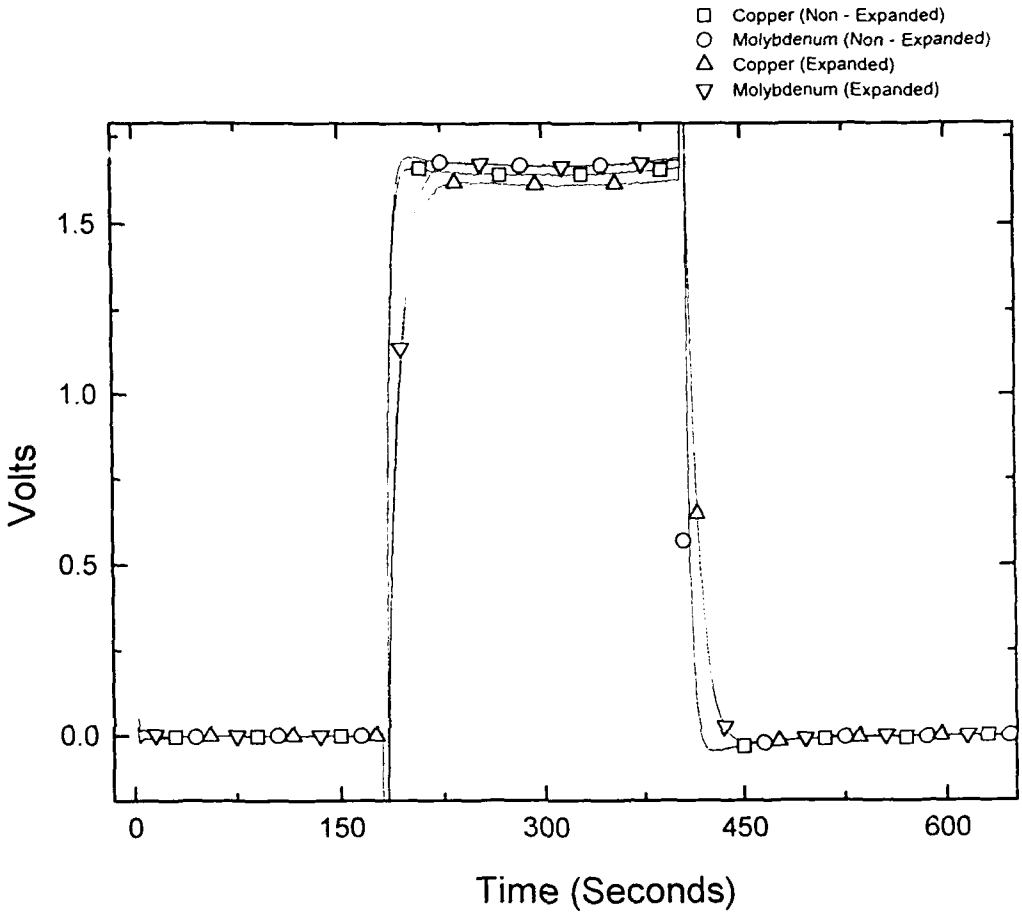

Figure. 22.

A graph of four heat capacity DSC scans. The difference in pan shape after pan expansion has led to longer time constants for the transient regions.

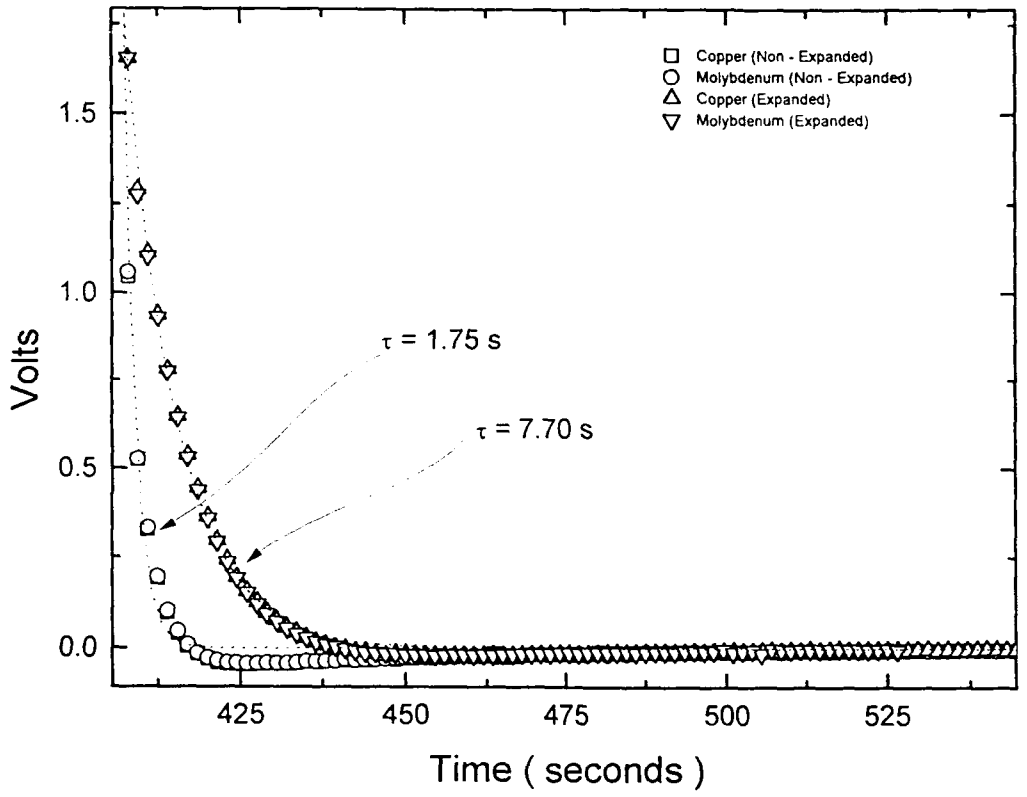

Figure. 23

A plot of the exponential decay to a baseline of two sets of heat capacity data. The time constants obtained from exponential fits of these two data sets can be used in Eq. 28 to compute the temperature lag for each of the scans. The difference between the two temperature lag between the expanded and non - expanded run is approximately 2 K.

lag would cause a 1.5% error in reported C_P, based upon the literature values of the specific heat of Cu.

And as a final note on the subject, the expansion of a pan will also cause an increase in the internal resistance of a powder sample because it is not packed as tightly as before the expansion. This change in pan shape could also cause a difference in the radiative and conductive heat losses of the pan. An interesting area for more study is to investigate the possibility of these differences in pan shape accounting for the level of the systematic error we have experienced in the higher temperature ranges.

Corrections for Sample Pan Mass Differences:

Another source of systematic error in DSC specific heat measurements is the differences in mass between the various sample pans. If the masses are not identical, the empty pan subtraction (Eq. 24) will not fully account for a portion of the DSC signal due to the sample's pan. This error becomes more pronounced as the number of moles in the sample decreases. Therefore the error is most prominent for small samples of high atomic mass because the pan will make a proportionally larger part of the signal. In the Dulong - Petit region, a 20mg Mo sample in a pan with a large variation of 1mg from the Al empty pan will produce a 17% variation in the measured heat content. For a similar Cu sample the variation will be 11%. If the mass of the samples is increased to 50mg, the errors drop to 5% for Cu and 7% for Mo. The best way to minimize the effects of this error is to use the largest sample size practical while maintaining small differences in pan mass.

It has been found practical to maintain a much smaller variation of $\pm$ .01mg in pan mass. For the samples and masses used in our measurements: Mo, ~ 80mg; Cu, ~ 50mg, and $TiSi_2$, ~ 30mg; based on Eq. 25, this variation in pan mass should cause an error of not more than .05% in any one sample run. However, a correction for pan mass difference based on Eq. 25 has been incorporated into our data analysis program.

$$\Delta Signal = \frac{\Delta Mass \cdot C_p \cdot R}{\mu \cdot F} \qquad \text{Eq. 29}$$

where:

$\Delta Signal$ = signal correction (volts)
$\Delta Mass$ = mass of the empty pan minus the mass of the sample pan (grams)
C_P = literature value of specific heat of pan material (Joules / mole · Kelvin)
R = heating rate (Kelvin / second)
F = calibration factor (Joules / Volt· Kelvin)
μ = molar mass of the pan material (grams/mole).

This difference in signal is then added to the empty pan signal to correct for the difference in mass. It should be noted, however, that this correction assumes the pan material is completely pure. Therefore, as mentioned earlier it is better to keep the differences in pan mass small than to rely on this correction. Fig. 24 is a plot of data analyzed with and without the correction.

It is important to note that although a variation in pan mass of ± .01mg could be maintained for a given box of pans (Perkin - Elmer part #0219 - 0062), there was a significant difference in the average pan mass between two different boxes, up to 1.5 mg. As previously discussed in this paper, this kind of variation could lead to significant errors for the unwary experimentalist.

There are many other factors that can affect specific heat measurements: purge gas, ice bath, etc. These topics are discussed in many sources.[20,31,32] The gist of the recommendations for minimizing errors due to these factors is: consistency. The most accurate specific heat measurements will be made by the experimentalist who is most consistent.

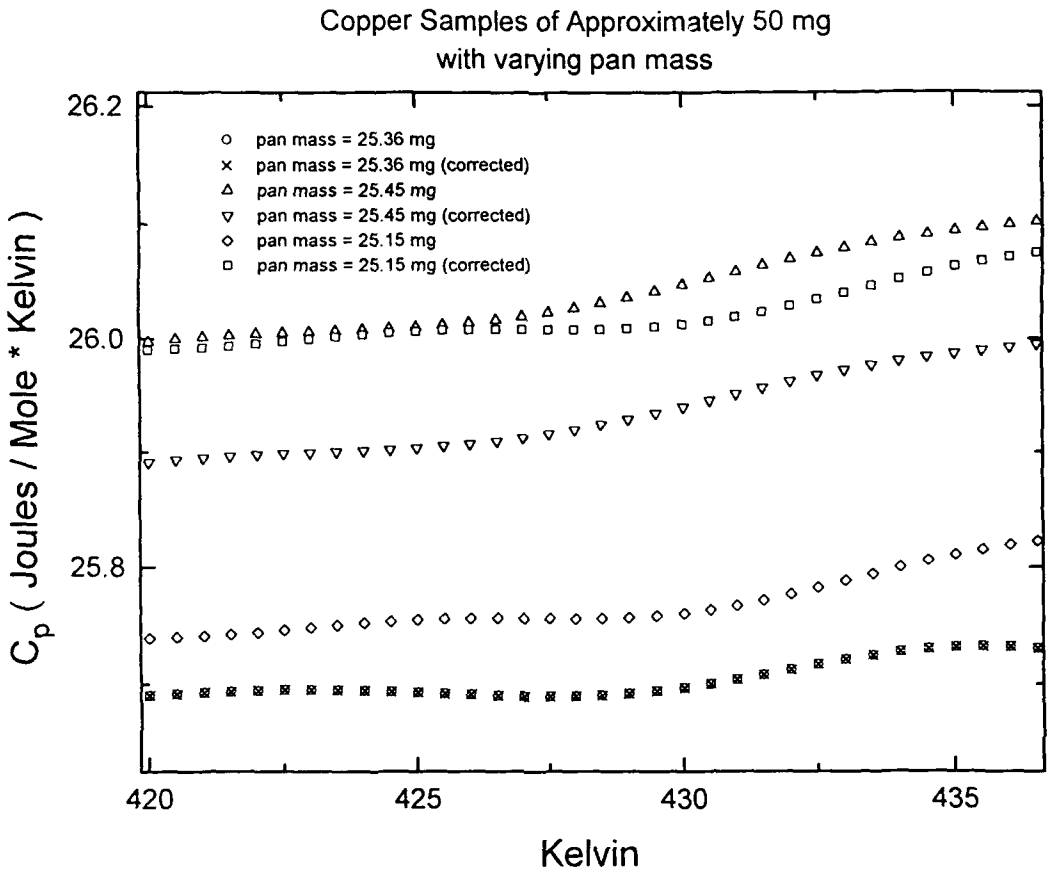

Figure 24.

A plot of three copper samples of about 50mg. The mass of the empty pan associated with these runs is 25.36mg. The mass of each of their pans is listed on the graph. Deviations in pan mass of this size should be avoided because this correction in not completely accurate.

Results and Conclusions:

All specific heat data obtained for $TiSi_2$ are plotted in Fig. 25 regardless of known detrimental influences or the known error in the data acquisition procedures. This data is presented not to be indicative what is believed to be the actual specific heat of $TiSi_2$, but to demonstrate some of the problems that can be encountered when measuring specific heat by DSC. The errors in the molybdenum runs associated with the data are contained in Fig. 26. It can be seen that there were severe problems with all measurements made above 500 K. The errors in these measurements are thought likely to be the effects of varying pan shape and varying particle size.

The specific heat data obtained after the samples were crushed to a fine powder and re-encapsulated are contained in Fig. 27. Also plotted in the figure are Golutvin's experimental data. There is a large discrepancy between our measured values and those of Golutvin. Because of the careful procedures followed in acquiring our data we feel our data are a better representation of the actual value of the specific heat of $TiSi_2$. Also our data show better agreement with accepted theory, Golutvin's data does not approach a Dulong - Petit value.

The error in the molybdenum runs associated with the data of Fig. 27 is contained in Fig. 28. The measured specific heat value of molybdenum is largely within $\pm$ 2% of its accepted value. Because an effort was made to match the total heat capacity and thermal resistances of molybdenum check sample and the $TiSi_2$ sample, it is believed that this error is indicative of the actual error in the $TiSi_2$ sample.

Our data, those of Golutvin, and the estimated values for the specific heat of $TiSi_2$ are plotted in Fig. 29. There is close agreement between our data and the estimated values. From this observation, it is clear that a Kopp's rule estimate for the specific heat of $TiSi_2$ is a valid approximation, and a better representation of the specific heat of $TiSi_2$ than Golutvin's data.

An approximate value of Debye temperature of $TiSi_2$ has been obtained by graphical means (Fig. 30). Because the lower limit of temperature range of the data is 100 K, this value is of limited credibility. The value of Θ_D that was estimated for $TiSi_2$ is about 510 ± 80 K. From this estimate a value of 22 ± 3 J/mole*K for the molar entropy at 298 K has been estimated.

The specific heat of $TiSi_2$ for room temperature values and above has been shown to be well behaved. That is to say, observed specific heat data agree well with predictions based upon a simple Debye model and estimates based upon the specific heat of its components, i. e., Ti and Si. These results justify, in the absence of experimental data, the approximation of the specific heat of $TiSi_2$ and hopefully the specific heats of the remainder of the Ti - Si compounds for use in the modeling of CVD reactions.

In conclusion, I would like to say that in order to accurately model the production of micro - electronic devices by the CVD of titanium disilicide, more data must be obtained. The specific heat functions of all products and reactants involved in the CVD process must be accurately known from absolute zero to the operating temperature of the CVD reactor. The data I have presented here are a beginning; hopefully these measurements will be expanded upon. The measurements should be continued to lower temperatures and expanded to include the entire Ti - Si phase diagram. Once these measurements have been obtained, the CVD of $TiSi_2$ can be optimized and will hopefully be used in production of the next generation of computers.

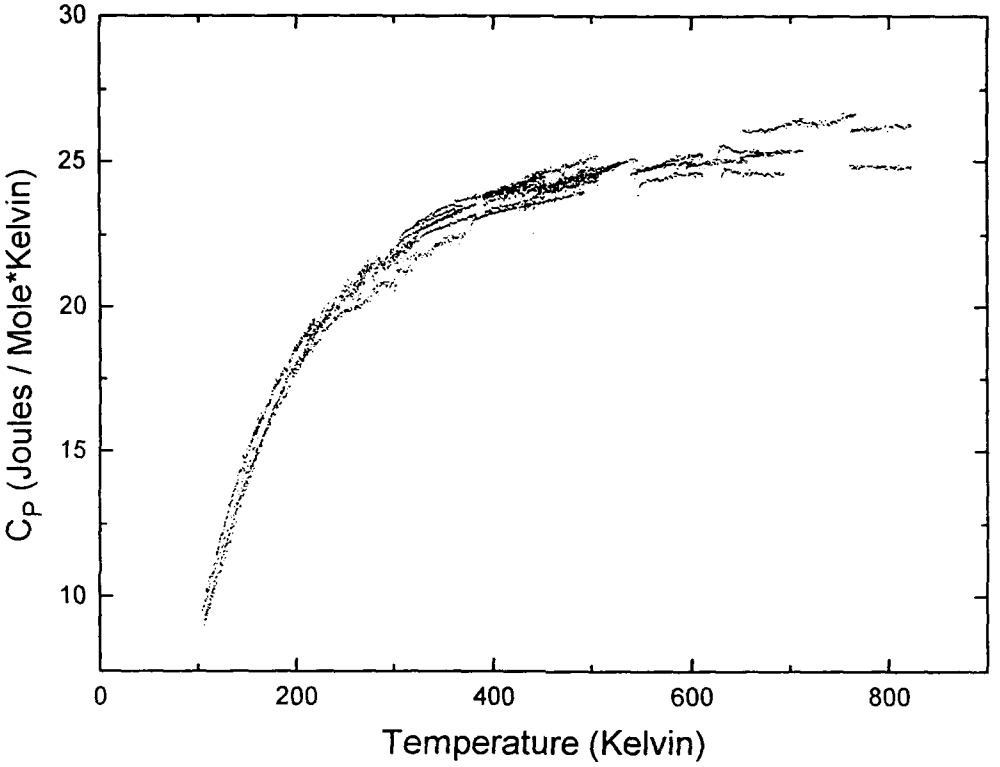

Figure. 25

A plot of all specific heat data for $TiSi_2$. This plot is included only as an exhibition of the problems that can be encountered while measuring specific heat by DSC.

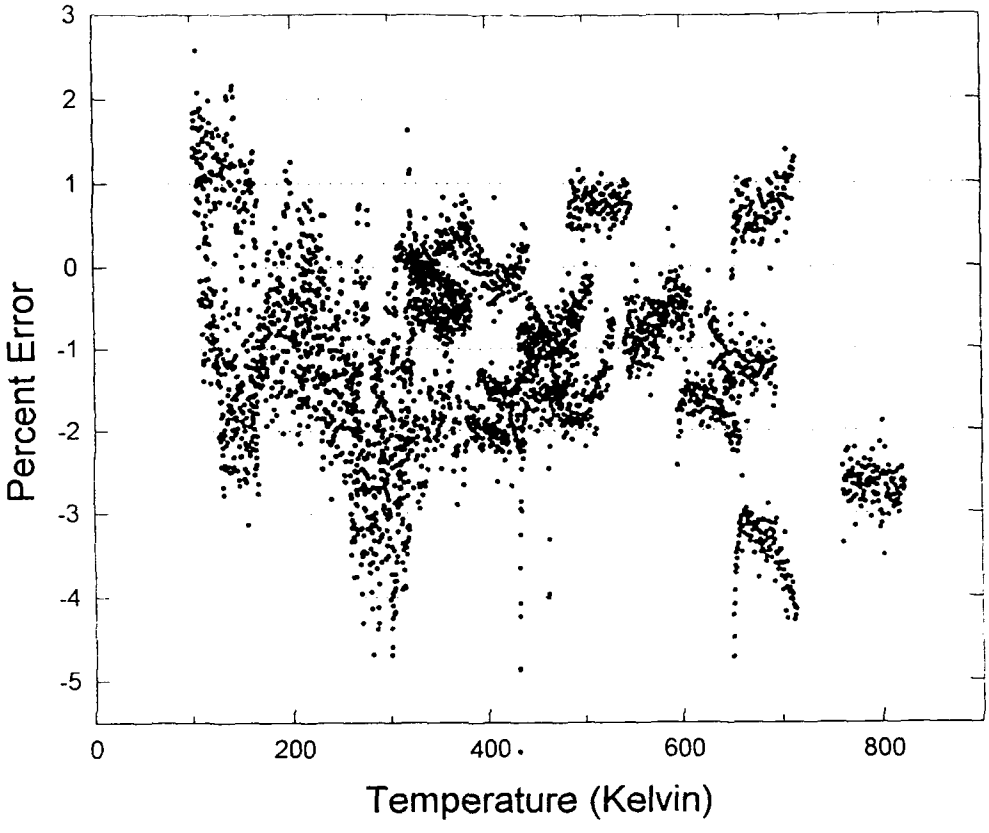

Figure. 26

A plot of the error in the molybdenum check associated with all $TiSi_2$ data.

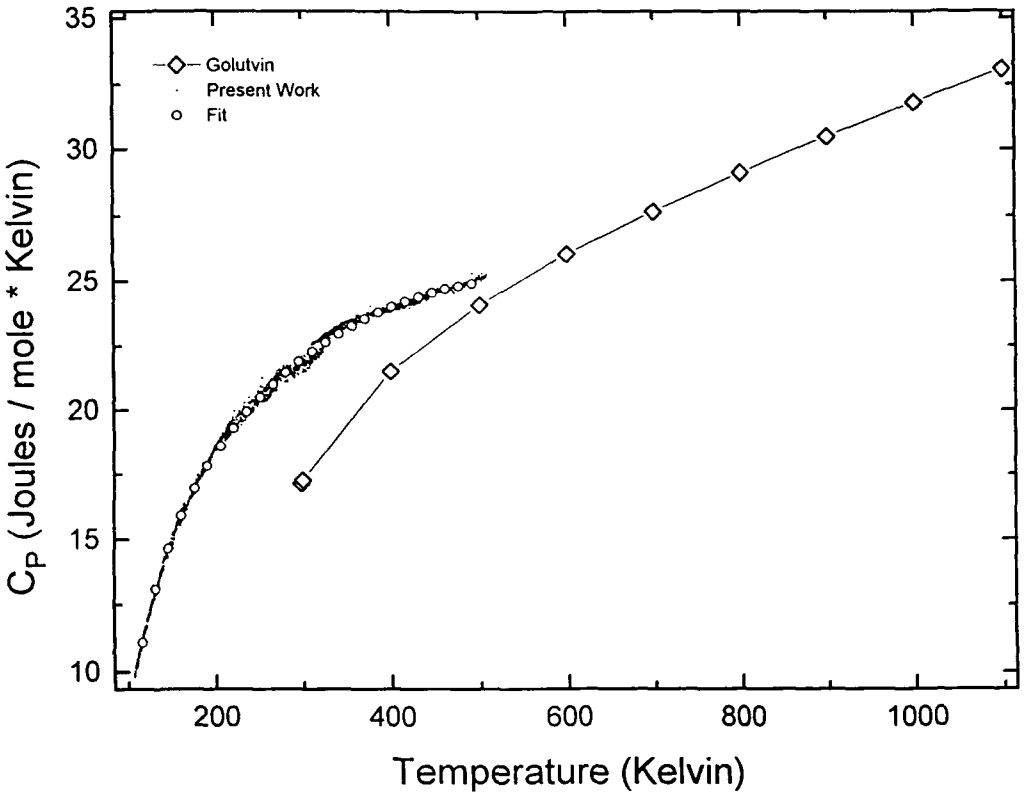

Figure. 27

A plot of the $TiSi_2$ data that we have accepted. Also plotted are Golutvin's data. A fit to the standard form of C_P from the literature was performed to yield: $C_P = 13.302 + .045079T - 92344T^{-2} - (4.2097 \times 10^{-5})T^2$. There is good agreement between the fit to the data and the data for the range of the experiment. However, the expression gives unrealistic values outside this data range.

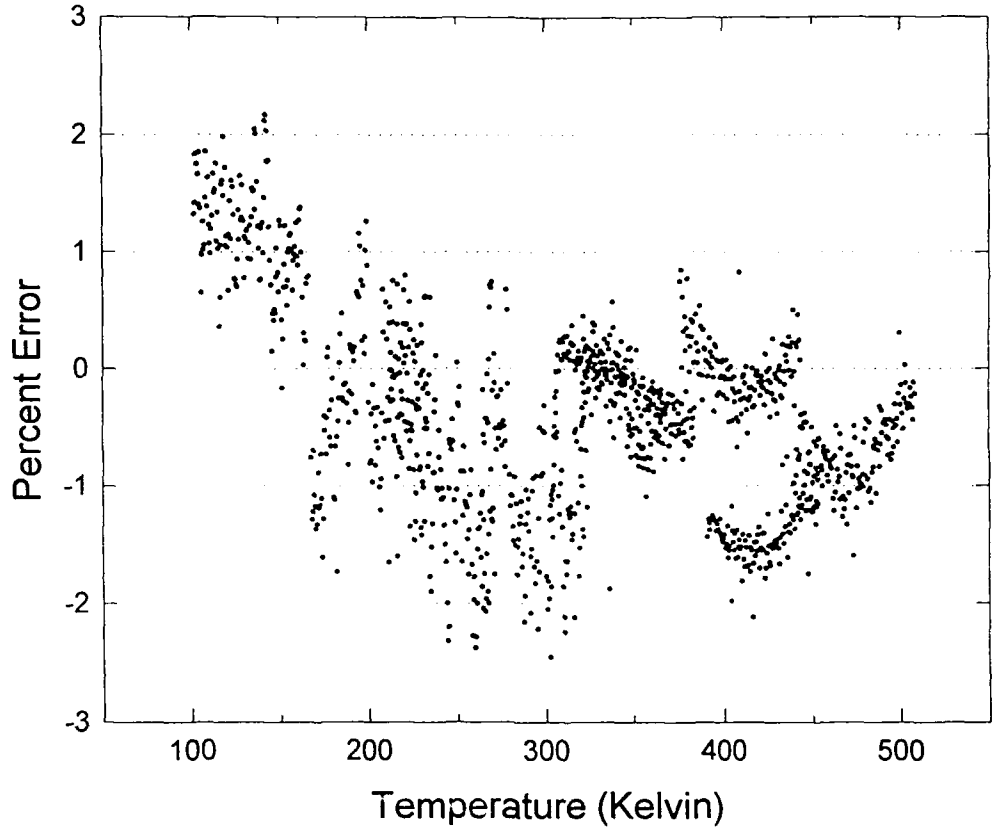

Figure. 28

The error associated with the $TiSi_2$ specific heat data. Some of the error in the low temperature data might be reduced when a new calibration for the DSC - 2 is obtained.

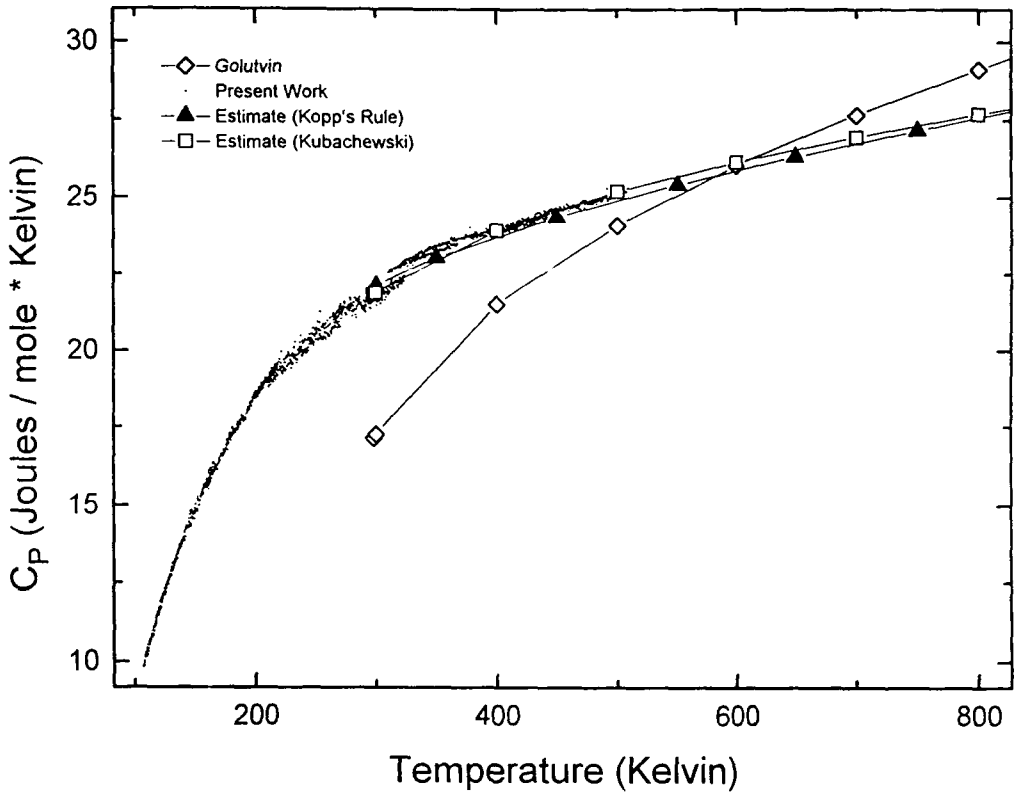

Figure. 29

A comparison of various values, estimated and experimental, of the specific heat of $TiSi_2$.

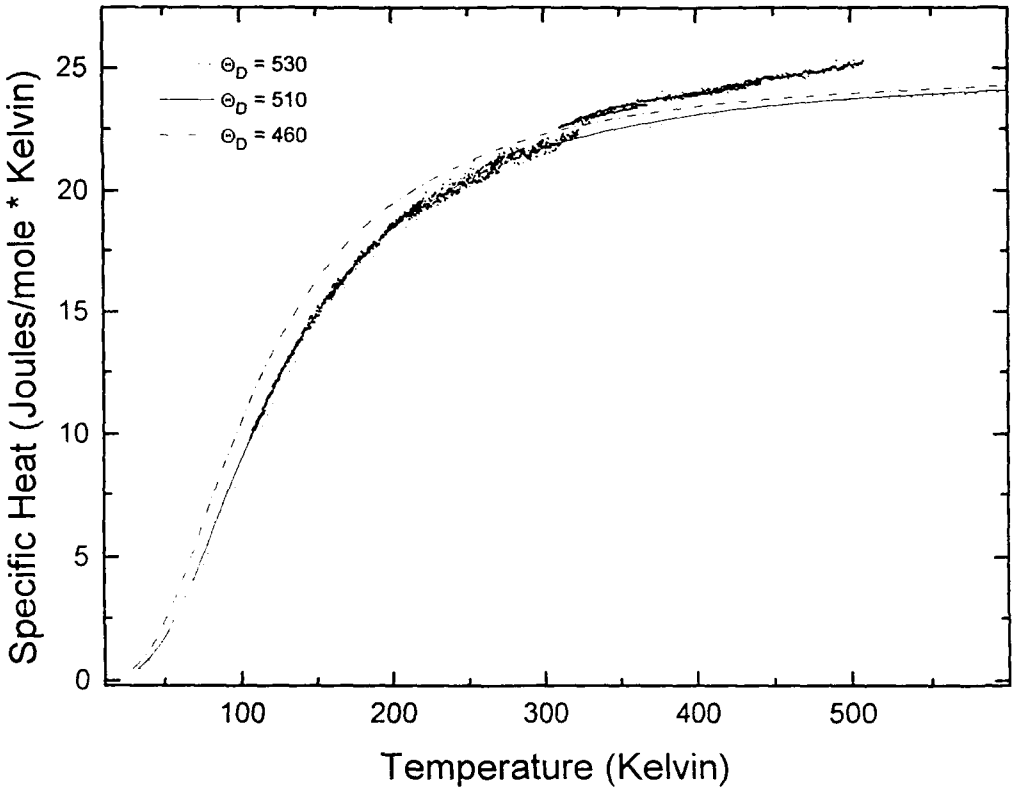

Figure. 30

Theta Debye was estimated for $TiSi_2$ by graphical means. More consideration was given to matching the low temperature values because C_P and C_V are closer in value at low temperatures. By this method an approximate value of Θ_D = 510 K was obtained. Also plotted are Debye curves for Θ_D = 460 K Θ_D = 530 K as references.

References

[1]Murarka, S. P. Silicides for VLSI Applications. Academic Press, New York, 98 (1983).

[2]Engqvist, J. *J. Electrochem. Soc.*, **139**, **11**, 3197 (1992).

[3]Bouteville, A., Attuyt, C., and Remy, J. C., *App. Surf. Sci.*, **53** 11 (1991)

[4]Madar, R. *Applied Surface Science*, **53**, 1 (1991).

[5]Golutvin, Y. M. *Russian Journal of Physical Chemistry*, **33**, **8**, 129 (1959).

[6]Bonderenko, V. P. *Poroshkovaya Metallurgiya*, **12, 168**, 49 (1976).

[7]Kubachewski, O. *Atomic Energy Review*, **9**, Vienna, 47 (1983).

[8]Schlesinger, M. E. *Chemical Reviews*, **90**, 607 (1990).

[9]Dulong, P. L. and Petit, A. T., *Ann. chim. phys.*, **10**, 395 (1819).

[10]Boltzmann, L., *Sitzb. kgl. Akad. Wiss. Wein*, **63:2**, 679 (1871).

[11]Chart, T. G. *National Physical Lab.*, Teddington, Rep. Chem., **18** (1972).

[12]Knacke, Kubachewski, O. Hesselman, . Thermochemical Properties of Inorganic Substances. Springer - Verlag. Berlin, 1991.

[13]Myers, H. P. Introductory Solid State Physics. Taylor & Francis. London, 1990

[14]Byrne, J. G., Recovery, Recrystallization, and Grain Growth. MacMillan, 65 (1965).

[15]AISN Software, *Jandel Scientific Peakfit*, (1992).

[16]National Inst. of Stand. and Tech., Standard Reference Material - 640b.

[17]Cullity, B. D. Elements of X- Ray Diffraction, Addison - Wesley, Reading, 350 (1978).

[18]Laves, F. Wallbaum, H. J. *Z. Kristallogr*, **101**, 78 (1939).

[19]Jeitschko, W. *Acta Cryst.*, **B33**, 2347 (1977).

[20]Patt, M. E., *Thermochimica Acta*, **197**, 413 (1992).

[21]National Inst. of Stand. and Tech., Reference Material - 5.

[22]Chase, M. W., Davies, C. A. and Downey, J. R. *J4NAF Thermochemical Tables*, **14**, 970 (1985).

[23]Furakawa, G. T., Saba, W. G., and Reilly, M. L., *NSRDS* **18** (1968).

[24]National Inst. of Stand. and Tech., Reference Material - 781 D1.

[25]Chase, M. W. et. al., *JANAF Thermochemical Tables*, **14**, 1508 (1985).

[26]Desai, P. D. *J. Phys. Chem. Ref. Data*, **16**, **1**, 91 (1987).

[27]Sacolik, I., *Thesis*, Suny Binghamton, (1991).

[28]Keithley Instruments Inc. *Asyst.* (1992).

[29]Perkin Elmer, *DSC - 2 Operators Manual*, 3-22 (1975).

[30]White, B. E., *Honors Thesis*, SUNY Binghamton, 20 (1990).

[31]Mraw, S. C. in Specific Heat of Solids, Ho, C. Y. ed. Hemisphere, New York, 395 (1988).

[32]Perkin Elmer, *DSC - 2 Operators Manual*, Chap 3 (1975).

Appendix 1

Contained in this appendix are Furukawa's selected values for the specific heat of Cu.[23] This selection is based upon the specific heat data for copper obtained by different experimentalists from 1914 to 1968. To obtain the values chosen, a least squares procedure to the experimental data was performed, giving more weight to the data they felt most accurate. Also included is a graph showing the percent deviation of the experimental data from their chosen value. On this graph they also give an estimated accuracy, but they do not say how they arrive at this estimate. For the part of the temperature range of our experiment for which data are presented, the accuracy is estimated to be better than 0.3%.

Gram atomic wt. = 63.5400, T °K = 273.15 + t °C, 1 cal = 4.1840 J

T	C_p°	$H_T^\circ - H_0^\circ$	$(H_T^\circ - H_0^\circ)/T$	S_T°	$-(G_T^\circ - H_0^\circ)$	$-(G_T^\circ - H_0^\circ)/T$
°K	*Cal/deg-mol*	*Cal/mol*	*Cal/deg-mol*	*Cal/deg-mol*	*Cal/mol*	*Cal/deg-mol*
1.00	0.000177	0.000086	0.000086	0.000258	0.000165	0.000165
2.00	0.000423	0.000378	0.000189	0.000451	0.000516	0.000258
3.00	0.000805	0.000978	0.000326	0.000689	0.00108	0.000360
4.00	0.00139	0.00206	0.000514	0.000995	0.00192	0.000479
5.00	0.00225	0.00385	0.000771	0.00139	0.00310	0.000620
6.00	0.00346	0.00668	0.00111	0.00190	0.00474	0.000790
7.00	0.00508	0.0109	0.00156	0.00255	0.00695	0.000994
8.00	0.00720	0.0170	0.00213	0.00336	0.00990	0.00124
9.00	0.00990	0.0255	0.00283	0.00436	0.0137	0.00153
10.00	0.0133	0.0370	0.00370	0.00557	0.0187	0.00187
11.00	0.0174	0.0523	0.00475	0.00702	0.0250	0.00227
12.00	0.0224	0.0721	0.00601	0.00874	0.0328	0.00274
13.00	0.0284	0.0974	0.00749	0.0108	0.0426	0.00327
14.00	0.0355	0.129	0.00923	0.0131	0.0545	0.00389
15.00	0.0439	0.169	0.0113	0.0159	0.0689	0.00459
16.00	0.0538	0.218	0.0136	0.0190	0.0863	0.00539
17.00	0.0651	0.277	0.0163	0.0226	0.107	0.00630
18.00	0.0783	0.348	0.0194	0.0267	0.132	0.00731
19.00	0.0933	0.434	0.0228	0.0313	0.161	0.00845
20.00	0.110	0.536	0.0268	0.0365	0.194	0.00972
25.00	0.230	1.363	0.0545	0.0729	0.460	0.0184
30.00	0.405	2.928	0.0976	0.130	0.958	0.0319
35.00	0.631	5.496	0.157	0.208	1.792	0.0512
40.00	0.894	9.296	0.232	0.309	3.077	0.0769
45.00	1.178	14.47	0.322	0.431	4.920	0.109
50.00	1.471	21.09	0.422	0.570	7.415	0.148
55.00	1.765	29.18	0.531	0.724	10.65	0.194
60.00	2.054	38.73	0.646	0.890	14.68	0.245
65.00	2.332	49.70	0.765	1.066	19.56	0.301
70.00	2.596	62.03	0.886	1.248	25.34	0.362
75.00	2.843	75.63	1.008	1.436	32.05	0.427
80.00	3.072	90.43	1.130	1.627	39.71	0.496
85.00	3.285	106.3	1.251	1.819	48.32	0.568
90.00	3.480	123.2	1.369	2.013	57.90	0.643
95.00	3.660	141.1	1.485	2.206	68.45	0.721
100.00	3.825	159.8	1.598	2.398	79.96	0.800
105.00	3.977	179.3	1.708	2.588	92.43	0.880
110.00	4.116	199.6	1.814	2.776	105.8	0.962
115.00	4.244	220.5	1.917	2.962	120.2	1.045
120.00	4.362	242.0	2.017	3.145	135.5	1.129
125.00	4.470	264.1	2.113	3.326	151.6	1.213
130.00	4.571	286.7	2.205	3.503	168.7	1.298
135.00	4.663	309.8	2.295	3.677	186.7	1.383
140.00	4.749	333.3	2.381	3.848	205.5	1.468
145.00	4.828	357.2	2.464	4.016	225.1	1.553

Gram atomic wt.=63.5400, T °K=273.15+t °C, 1 cal=4.1840 J

T	C_P°	$H_T^\circ - H_0^\circ$	$(H_T^\circ - H_0^\circ)/T$	S_T°	$-(G_T^\circ - H_0^\circ)$	$-(G_T^\circ - H_0^\circ)/T$
°K	Cal/deg-mol	Cal/mol	Cal/deg-mol	Cal/deg-mol	Cal/mol	Cal/deg-mol
150.00	4.901	381.6	2.544	4.181	245.6	1.638
155.00	4.969	406.3	2.621	4.343	266.9	1.722
160.00	5.032	431.3	2.695	4.502	289.1	1.807
165.00	5.090	456.6	2.767	4.658	312.0	1.891
170.00	5.145	482.2	2.836	4.811	335.6	1.974
175.00	5.196	508.0	2.903	4.960	360.1	2.058
180.00	5.244	534.1	2.967	5.107	385.2	2.140
185.00	5.289	560.4	3.029	5.252	411.1	2.222
190.00	5.331	587.0	3.089	5.393	437.7	2.304
195.00	5.371	613.8	3.147	5.532	465.1	2.385
200.00	5.408	640.7	3.203	5.669	493.1	2.465
205.00	5.443	667.8	3.258	5.803	521.7	2.545
210.00	5.476	695.1	3.310	5.934	551.1	2.624
215.00	5.507	722.6	3.361	6.064	581.1	2.703
220.00	5.537	750.2	3.410	6.191	611.7	2.781
225.00	5.565	778.0	3.458	6.315	643.0	2.858
230.00	5.591	805.8	3.504	6.438	674.9	2.934
235.00	5.616	833.9	3.548	6.558	707.4	3.010
240.00	5.640	862.0	3.592	6.677	740.5	3.085
245.00	5.663	890.3	3.634	6.793	774.1	3.160
250.00	5.684	918.6	3.675	6.908	808.4	3.234
255.00	5.704	947.1	3.714	7.021	843.2	3.307
260.00	5.722	975.7	3.753	7.132	878.6	3.379
265.00	5.740	1004.	3.790	7.241	914.5	3.451
270.00	5.757	1033.	3.826	7.348	951.0	3.522
273.15	5.767	1051.	3.848	7.415	974.2	3.567
275.00	5.773	1062.	3.861	7.454	988.0	3.593
280.00	5.788	1091.	3.896	7.558	1026.	3.663
285.00	5.803	1120.	3.929	7.661	1064.	3.732
290.00	5.818	1149.	3.961	7.762	1102.	3.800
295.00	5.832	1178.	3.993	7.862	1141.	3.868
298.15	5.840	1196.	4.013	7.923	1166.	3.911
300.00	5.845	1207.	4.024	7.960	1181.	3.936

H_0° is the enthalpy of the solid at 0 °K and 1 atm pressure.

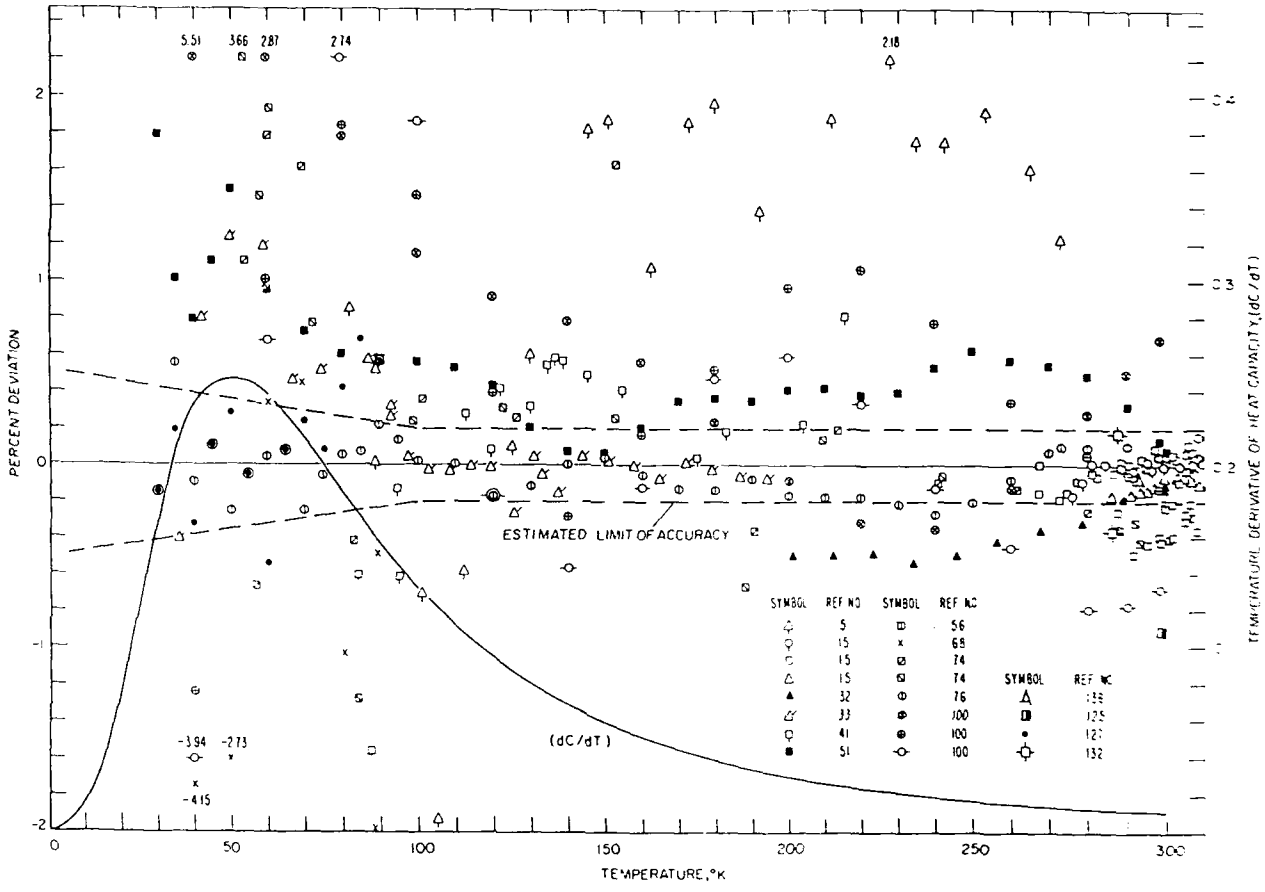

FIGURE 2a. *Deviations of the heat-capacity data of the literature on copper from the selected values in the range 30 to 300 °K. The estimated limit of accuracy and the temperature derivative, dC/dT, in J °K⁻¹ mol⁻¹ of the selected values.*

Appendix 2

Contained in this appendix are Desai's selected values for the specific heat of Mo.[26] This selection is based upon the specific heat data for molybdenum available through 1985. Desai does not discuss the methods used to arrive at these values. A graph of Desai's selected value for low temperature and the data used to used in its determination is included. Also contained is a graph of the deviations between the selected value and the experimental results. Desai reports deviations of $\pm$ 1.5% to $\pm$ 3% between his selection and the experimental data.

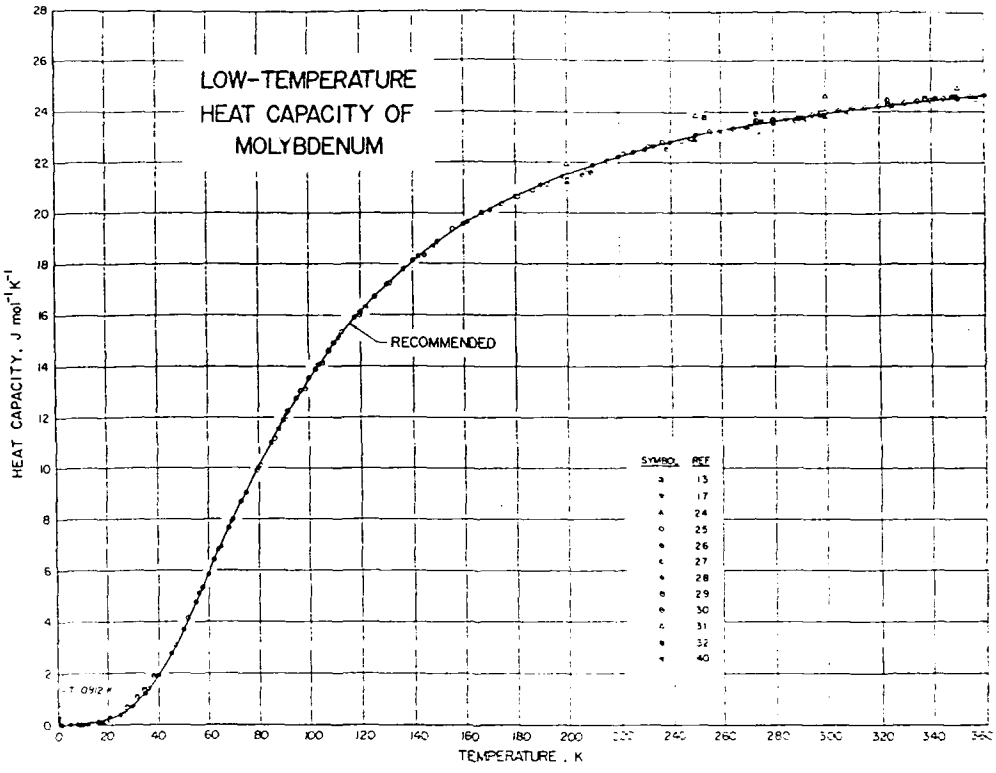

Fig. 3. Low-temperature heat capacity of molybdenum.

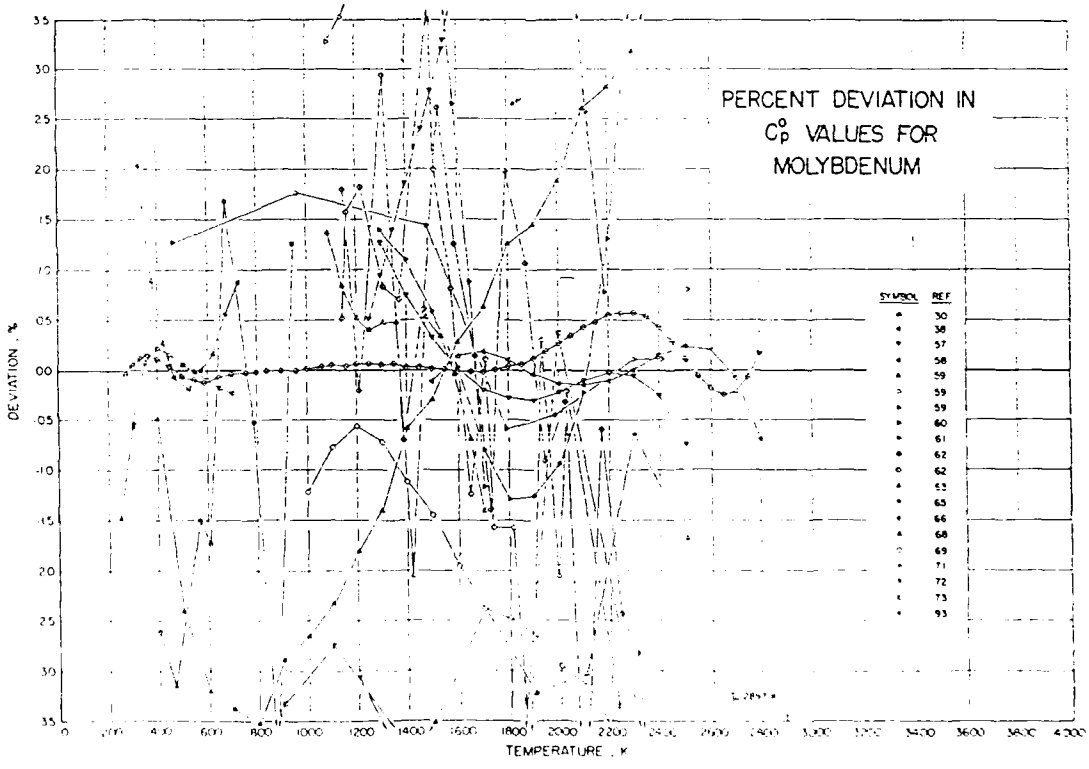

Table 9. Recommended low-temperature heat capacity of molybdenum

T / K	C°_p / J·mol^{-1}·K^{-1}		T / K	C°_p / J·mol^{-1}·K^{-1}
0.4	0.000544[a]	0.000741[b]	90	11.910
0.5	0.00109[a]	0.000928[b]	100	13.498
0.6	0.00169[a]	0.00112[b]	110	14.875
0.8	0.00305[a]	0.00149[b]	120	16.101
0.912	0.00395[a]	0.00171[b]	125	16.658
1	0.00187		130	17.178
2	0.00390		140	18.099
3	0.00621		150	18.889
4	0.00896		160	19.571
5	0.0121		170	20.154
6	0.0156		175	20.420
7	0.0194		180	20.662
8	0.0237		190	21.113
9	0.0284		200	21.521
10	0.0341		210	21.890
15	0.0834		220	22.228
20	0.213		225	22.388
25	0.428		230	22.540
30	0.770		240	22.821
35	1.265		250	23.064
40	1.909		260	23.275
50	3.698		270	23.461
60	5.912		273.15	23.515
70	8.019		280	23.626
75	9.112		290	23.777
80	10.094		298.15	23.900

[a] Superconductor
[b] Nonsuperconductor in magnetic field

$$C_{(electronic)} = \gamma T \qquad \gamma = 1.85 \pm 0.02 \text{ mJ·mol}^{-1}\text{·K}^{-2}$$

Table 14. Recommended high-temperature thermodynamic properties of molybdenum[a]

	Condensed Phase				Gas Phase Mo(g)			
T / K	C°_p / J·mol^{-1}·K^{-1}	$H^\circ-H^\circ(Tr)$ / J·mol^{-1}	S° / J·mol^{-1}·K^{-1}	$-[G^\circ-H^\circ(Tr)]/T$ / J·mol^{-1}·K^{-1}	C°_p / J·mol^{-1}·K^{-1}	$H^\circ-H^\circ(Tr)$ / J·mol^{-1}	S° / J·mol^{-1}·K^{-1}	$-[G^\circ-H^\circ(Tr)]/T$ / J·mol^{-1}·K^{-1}
298.15	23.900	0	0.000	28.592	20.786	0	0.000	181.841
300	23.918	44	0.148	28.592	20.786	38	0.129	181.841
350	24.555	1257	3.884	28.886	20.786	1078	3.332	182.093
400	25.078	2498	7.198	29.546	20.786	2117	6.109	182.657
450	25.507	3763	10.177	30.408	20.786	3156	8.556	183.383
500	25.874	5047	12.884	31.382	20.786	4196	10.747	184.197
550	26.192	6349	15.366	32.414	20.786	5235	12.727	185.050
600	26.470	7666	17.657	33.472	20.786	6274	14.537	185.921
650	26.721	8996	19.785	34.538	20.786	7314	16.199	186.789
700	26.960	10338	21.775	35.598	20.786	8353	17.741	189.649
750	27.197	11692	23.643	36.646	20.786	9392	19.174	188.492
800	27.432	13057	25.405	37.676	20.786	10431	20.517	189.318
850	27.671	14435	27.076	38.685	20.786	11471	21.775	190.121
900	27.905	15824	28.664	39.673	20.786	12510	22.965	190.906
950	28.139	17226	30.179	40.639	20.786	13549	24.087	191.666
1000	28.380	18638	31.628	41.582	20.787	14589	25.155	192.407
1100	28.900	21502	34.357	43.402	20.788	16667	27.136	193.825
1200	29.481	24420	36.896	45.116	20.793	18747	28.945	195.164
1300	30.129	27400	39.281	46.796	20.803	20826	30.610	196.431
1400	30.849	30449	41.540	48.383	20.823	21907	32.152	197.632
1500	31.647	33573	43.695	49.905	20.856	24991	33.590	198.770
1600	32.500	36780	45.764	51.369	20.910	27079	34.938	199.854
1700	33.398	40074	47.761	52.780	20.989	29174	36.207	200.887
1800	34.367	43462	49.697	54.144	21.100	31278	37.410	201.874
1900	35.145	46951	51.583	55.464	21.250	33395	38.555	202.819
2000	36.540	50548	53.428	56.746	21.443	35530	39.649	203.726
2100	37.748	54261	55.240	57.993	21.687	37686	40.701	204.597
2200	39.074	58102	57.026	59.208	21.985	39869	41.717	205.436
2300	40.503	62079	58.794	60.395	22.342	42085	42.702	206.245
2400	42.058	66206	60.550	61.556	22.761	44339	43.661	207.028
2500	43.830	70499	62.302	62.693	23.248	46639	44.600	207.785
2600	45.900	74982	64.060	63.813	23.802	48991	45.522	208.521
2700	48.390	79692	65.838	64.914	24.428	51402	46.432	209.235
2800	51.485	84681	67.651	66.000	25.127	53892	47.333	209.931
2897(s)	55.058	89844	69.462	67.042	25.870	56430	48.228	210.610
2897(l)	40.350	128944	82.959	67.042	25.870	56430	48.228	210.610
3000	40.350	133100	84.369	68.594	26.742	59061	49.120	211.274
3200	40.350	141170	87.073	71.449	28.647	64595	50.903	212.560
3400	40.350	149240	89.419	74.117	30.827	70538	52.706	213.800
3600	40.350	157310	91.725	76.620	33.356	76943	54.536	215.004
3800	40.350	165380	93.907	78.978	35.900	83855	56.404	216.178
4000	40.350	173450	95.977	81.206	38.713	91314	58.316	217.328
4200	40.350	181520	97.945	83.318	41.649	99349	60.275	218.462
4400	40.350	189590	99.822	85.326	44.658	107978	62.282	219.583
4600	40.350	197660	101.616	87.238	47.696	117214	64.334	220 694
4800	40.350	205730	103.333	89.065	50.725	127055	66.428	221.799
4983	40.350	213114	104.843	90.667	53.461	136589	68.376	222.806
5000	40.350	213800	104.981	90.813	53.713	137500	68.558	222.899

Appendix 3

The calibration factors for the DSC -2 and DSC - 4.

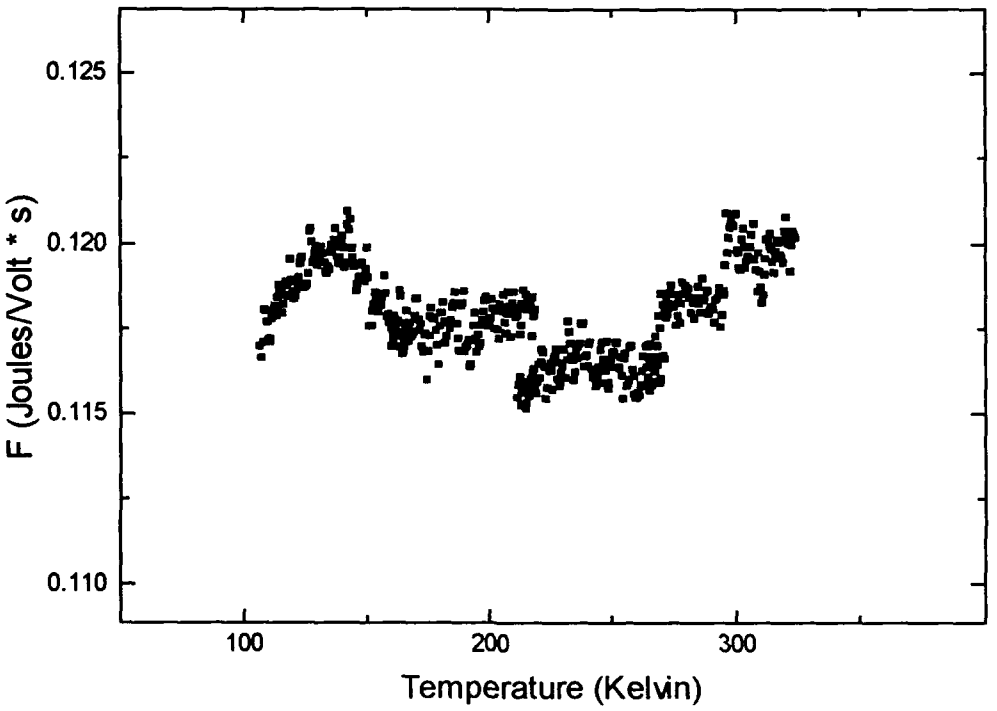

The calibration factor for the DSC - 2.

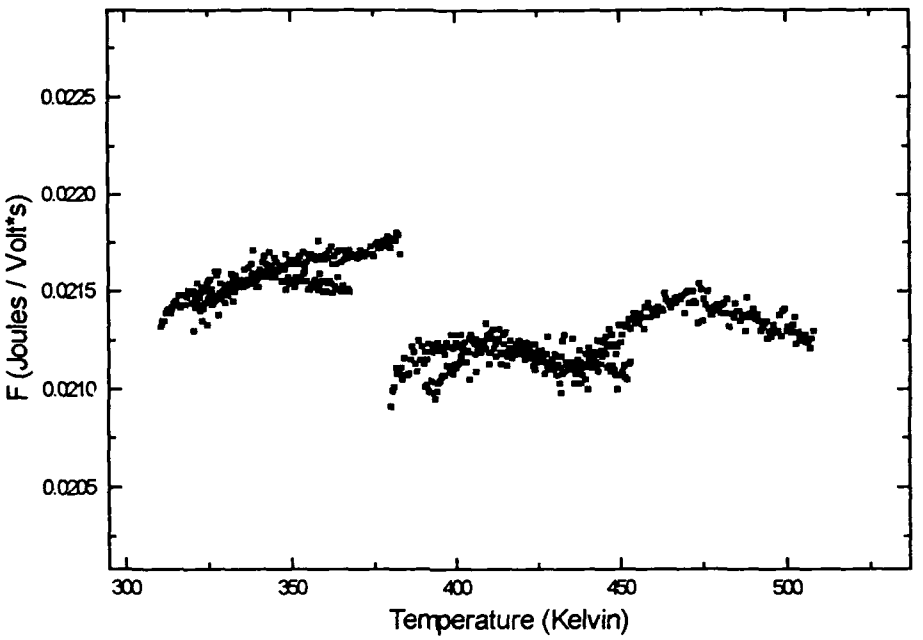

The calibration factor for the DSC - 4.